FORCE CHAINS AND THE FRAGMENTATION OF GRANULAR MATERIALS

by

Yojiro Yoshida

B. S. in Civil Engineering, University of Pittsburgh, 2003

Submitted to the Graduate Faculty of

School of Engineering in partial fulfillment

of the requirements for the degree of

Master of Science

University of Pittsburgh

2004

UNIVERSITY OF PITTSBURGH

SCHOOL OF ENGINEERING

This thesis was presented

by

Yojiro Yoshida

It was defended on

November 2, 2004

and approved by

Luis E. Vallejo, PhD, Professor

Jeen-Shang Lin, PhD, Associate Professor

Julie M. Vandenbossche, PhD, Assistant Professor

Thesis Advisor: Luis E. Vallejo, PhD, Professor

ABSTRACT

FORCE CHAINS AND THE FRAGMENTATION OF GRANULAR MATERIALS

Yojiro Yoshida, M.S.

University of Pittsburgh, 2004

In this study, the fragmentation of granular materials is evaluated by laboratory experiments and by numerical and theoretical analyses. The laboratory experiments used were the direct shear, point load, compaction, and grain size distribution tests. The Discrete Element Method (DEM) was used for the numerical analysis. Fractal theory was used to interpret the laboratory results. The direct shear tests were carried out on wooden cylindrical rods. These tests and its DEM simulation indicated that the normal and shear loads exerted by the direct shear equipment were transmitted and resisted by the rods through force chains. Only a fraction of the rods developed these resisting force chains, the rest of the rods remained idle and could be removed without affecting the stability of the system. The effect of force chains on the simulated granular material was studied in the laboratory by the point load test. Point load tests on gravel indicated that the size of the gravel and their degree of moisture influenced their strength. Proctor tests were also used to analyze fragmentation under compressive loads. Samples of gravel were subjected to different levels of compression in a cylindrical container measuring 10 cm in diameter. DEM simulation of the test indicated that the compressive force induced by the Proctor hammer was transmitted to the gravel through force chains. These force chains caused the fragmentation of the gravel. The grain size distribution of the gravel before and after the compaction tests were

evaluated and used in conjunction with fractal theory to analyze the levels of fragmentation experienced by the gravel. The fragmentation fractal dimension was used to evaluate the changes in size distribution experienced by the gravel. The fragmentation fractal dimension was found to increase with the degree of fragmentation of the gravel. Changes in the shape of the gravel particles as a result of their fragmentation were evaluated using fractal theory. Thus, the fractal dimension concept from fractal theory was found to be a simple and powerful theoretical tool to analyze the changes experienced by granular materials as a result of their fragmentation.

TABLE OF CONTENTS

Page

LIST OF TABLES

Page

LIST OF FIGURES

Page

ACKNOWLEGEMENTS

I would like to show my gratitude to many people who helped me writing this thesis. I would like to thank: Dr. Luis E. Vallejo, for guiding me through this research; Mrs. Nancy Downes for editing this paper; and my friend and colleague Mr. Sebastian Lobo-guerrero for countless advices.

1.0 INTRODUCTION

The purpose of this research is twofold: to determine the transmission of force through granular materials and to study the fracture of granular materials under applied force. When a mass of granular material is under stress, this force is transmitted throughout the material by particle contact. This chain of continuous contact between particles is known as a “force chain”. A force chain transmits both shear and compressive forces through the particles that form it. Thus, a force chain causes particles to fracture either at their surface (abrasion) or through the body of the individual particles (fragmentation).

For this research, several different types of tests were performed to study the behaviors of granular materials. Point load tests were performed to simulate and observe the effect of force chains on the fragmentation of the particles. Then, proctor tests were performed with various numbers of blow counts to determine the effect of force on abrasion and fragmentation. Direct shear tests on simulated granular materials were also conducted to understand how force chains are transmitted through granular materials.

Fractal theory was used to analyze the fragmentation of particles since the roughness of particle surfaces have an important effect on the behavior of granular materials. The size distribution of materials also has an important effect on the material’s behavior. The usefulness of conventional approaches to analyze particle roughness and size distribution are limited due to

their methodologies. However, using fractal theory to analyze both the roughness and size distribution of the particles can help determine these parameters with greater accuracy.

2.0 MECHANICS OF FRAGMENTATION OF GRANULAR MATERIAL

There are many factors influencing the fragmentation of a granular particle; coordination number, particle size, and applied stress are the main ones. In addition, the type of fracture must be considered in order to fully understand the crushing behavior, which produces fragmentation.

2.1 COORDINATION NUMBER

The coordination number is the number of contacts a particle has with adjacent particles. This number serves as an important parameter in describing the geometrical arrangement of particles in a packing. It has also been widely used in evaluating structural properties related to the connectivity between particles, including force transmission and tensile strength.

Pinson, Zou, Yu, Zulli and McCarthy [(1)] studied the number of contact points between particles by using steel ball. Their results suggest that in the sphere containing grains of the same size, the overall coordination number was 6.24. However, in order to represent the actual situation in the field, the data based solely on particles of a single particle size is insufficient to represent the complex nature of natural granular material. Thus, the same experiment was subsequently performed using a binary mixture of steel balls of two different sizes. For a binary mixture of steel ball (large size and small size), there are different types of contacts: small-to-small, small-to-large, large-to-small, and large-to-large. The coordination number for large

particles is the sum of large-to-small and large-to-large contacts and the coordination number for small particles is the sum of small-to-small and small-to-large contacts. The summarized results of this second experiment are shown in Figure 2.1 and 2.2. These figures show the change in coordination number with respect to the change of the volume ratio of small balls. Figure 2.1 is the plot for the small-to-large size ratio of 1:2 and Figure 2.2 is the plot for small-to-large size ratio of 1:4.

In a binary mixture of particles, there are two factors influencing the coordination number: a statistical factor and a geometric factor. When volume fraction of particles of a particular size increases, the number of contacts between this same sized particles increases. This is because when there are more particles of the same size, a particle's chance of having a neighbor of that same size increases. The influence of this statistical factor can be seen in both plots of Figure2.1 and 2.2, which shows that as the volume fraction of small particles increases, the number of small-to-small contacts also increases. With a decrease in the volume fraction of small particles, or an increase in the volume fraction of large particles, the number of large-to-large contacts also increases.

The second factor that influences the number of contacts is the geometric factor. In a binary mixture, large particles should have a higher coordination number than small particles because of their larger surface area. For the same reason, small particles should have a lower coordination number. In Figure 2.1 and 2.2, the plot of the coordination number representing the large-to-small contacts shows that particle in most cases, the number of large-to-small contacts is much higher than the number of small-to-large contacts. The only exception is when the volume fraction of small particles is less than 8%. At this phase, the number of small-to-large contacts is

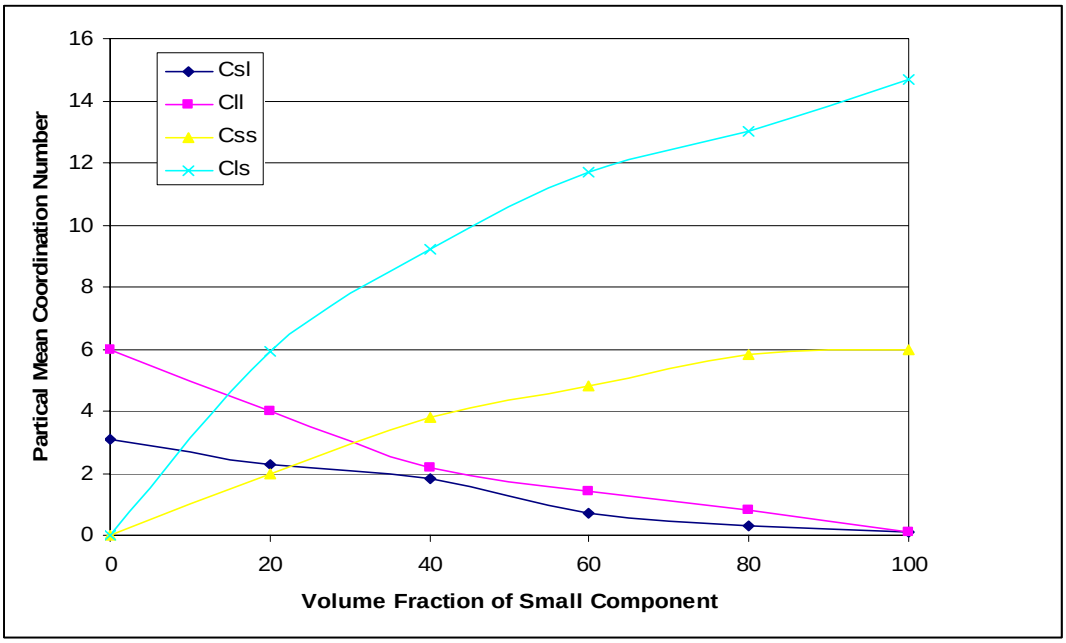

Figure 2.1: Mean coordination numbers for binary sphere packing when the small-to-large size ratio is 1:2.
(modified from Pinson et al. [1])

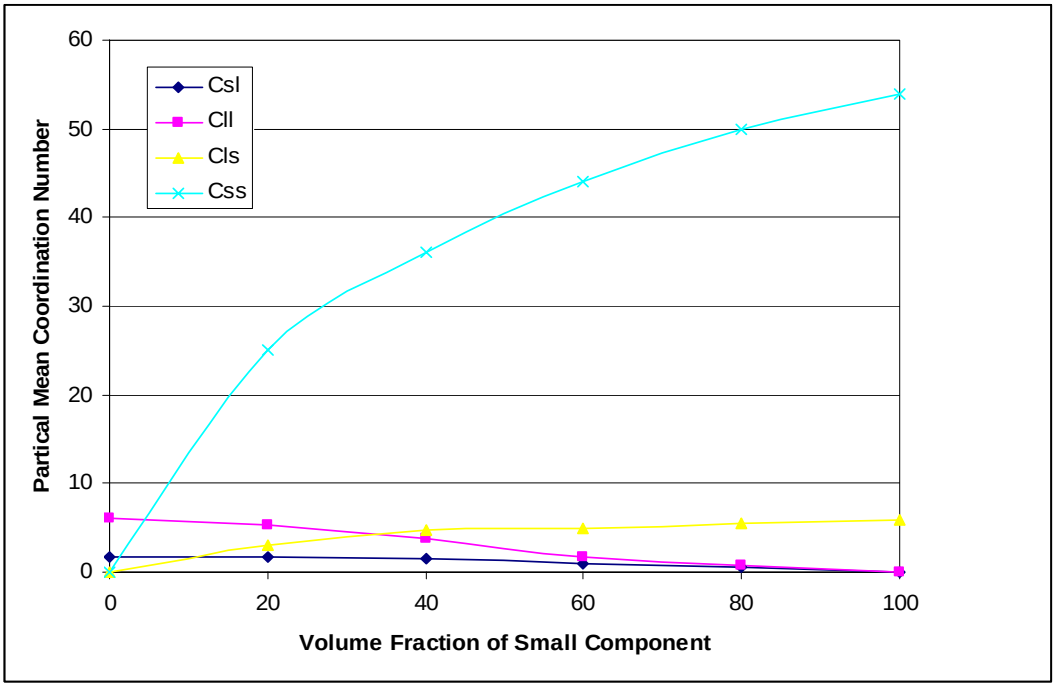

Figure 2.2: Mean coordination numbers for binary sphere packing when the small-to-large size ratio is 1:4.
(modified from Pinson et al. [1])

higher than the number of large-to-small contacts. But at the same time, the number of large-to-large particle contacts is high at this phase. Thus, a large particle ends up having a higher coordination number than a small particle. By comparing the number of large-to-small contacts in Figure 2.1 and 2.2 another influencing geometric factor can be seen.

As mentioned above, the trend for change in the number of large-to-large contacts and small-to-small contacts is similar for both plots of Figure 2.1 and 2.2. This means that these two types of contacts are governed primarily by the statistical factor and that there is not much geometric influence.

As a result, increasing the volume fraction of small particle components increases the small-to-small and large-to-small contacts but decreases the small-to-large and large-to-large contacts. This result also shows that although there are two factors, statistical and geometrical, that influence the coordination number, the geometrical factor has a greater influence on the total coordination number.

When a particle is in contact with surrounding particles, these contacts work as support. Thus, a higher coordination number indicates that the force is distributed through contacting particles to a higher degree. This phenomenon also reduces the stress on the particle, causing a higher chance of the particles surviving the impact.

2.2 PARTICLE SIZE

Particle size is another important factor that greatly influences the failure of granular material, and much research has dealt with the correlation of particle size and strength.

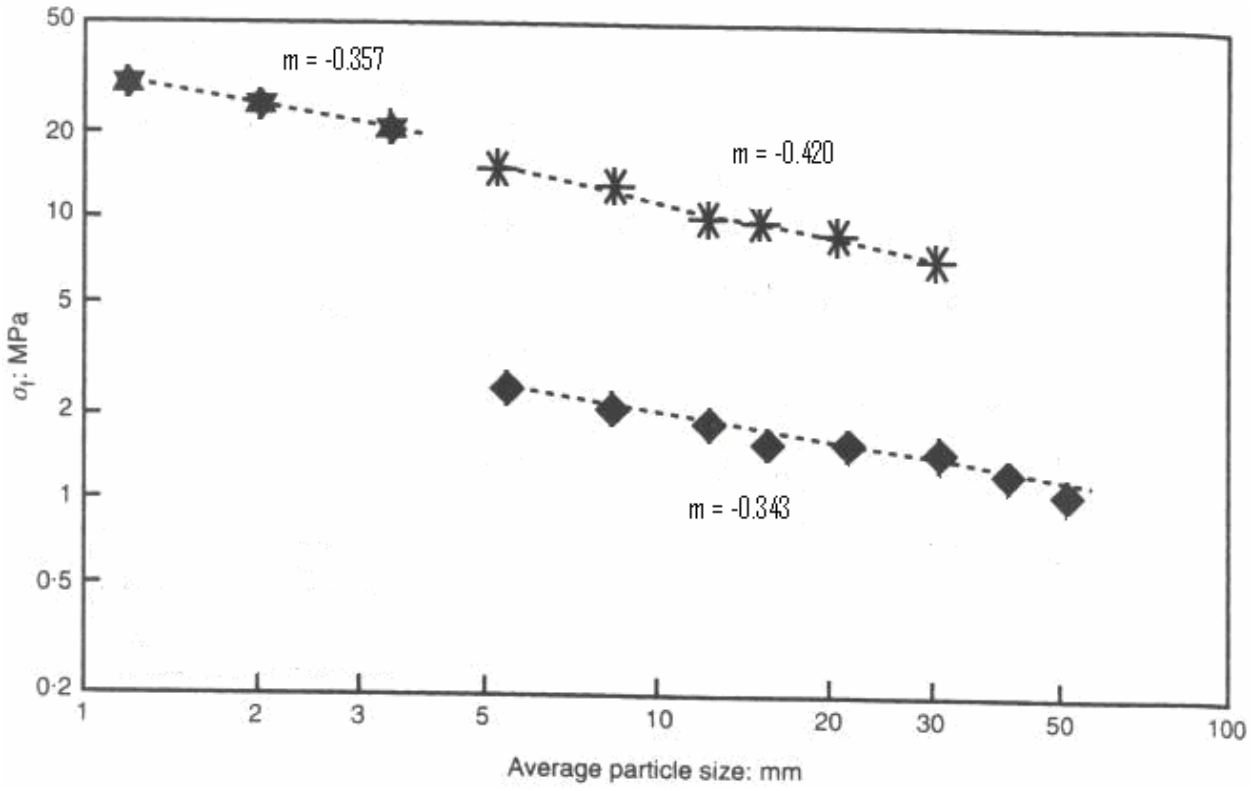

Figure 2.3: Average particle size and tensile strength of particle.
(modified from McDowell and Bolton [2])

Lee studied the relationship between particle diameter and tensile strength of three different types of granular materials [2] and found the results, which are presented in Figure 2.3 above. Although the slopes of the plots for each material are different, the relationship between strength and particle size is evident. For all three types of particles, strength decreases proportionally as

diameter increases. One factor that causes this phenomenon is a flaw in the body of a particle [3]. A flaw is a defect or tiny crack that exists in the body of granular material and is distributed throughout the body of a particle. The crack, which causes the final fracture of the particle, propagates through this flaw. On contrarily to a big particle, a small particle has fewer flaws due to its smaller body size. Also, since a smaller particle is often a fragment of a larger particle and since large flaws tend to be the ones that cracks propagate through, a small particle generally contains fewer smaller flaws. These factors make smaller particles stronger than bigger particles. This theory will be further discussed with the results of the point load test in Chapter 5.

2.3 TYPE OF FRACTURE

The two main categories used to classify crushing are abrasion and fragmentation. Abrasion describes the fracture of a particle only at the surface whereas fragmentation describes the fracture of the body of a particle. Fragmentation causes the body of a particle to split into 2 or more pieces and thus it is often considered as the total failure of particle. On the other hand, abrasion of a material is only a fracture of the material's surface and so it is not considered as total failure.

Nakata, Hyde, Hyodo, and Murata [4] have categorized the failure of particles into three types. Type 1 failure occurs when only the surface of the particle is fractured. Thus, type 1 failure is equivalent to abrasion of a particle. Type 2 failure occurs when the major asperities of a particle are crushed or fragmented. And type 3 failure occurs when a particle is split into 2 or more pieces. It should be noted that although Type 2 failure can be categorized as either abrasion

or fragmentation, but since it has the characteristics of both, it is generally distinguished from Type 1 and 3.

3.0 FRACTAL ANALYSIS

A fractal is an irregularity or fragmented shape of a geometrical or physical structure that is identical at any scale of measurement to a larger pattern of which it is part. In this research, fractal theory was used to quantify features such as roughness or size distribution of particles. Fractal theory [5] can be used to analyze the roughness and the size distribution of particles, and the result can be quantified. These two parameters greatly influence the behavior of soil mass. For example, it was found that roughness influences an internal friction angle [6]. Much research has been performed and many different methodologies have been developed in order to measure roughness and size distribution to date.

3.1 OTHER SHAPE ANALYSIS

There are many methods to measure the roughness of particles; visual comparison is one of the most widely used. With this method, a particle is compared to standard charts of different criteria such as roughness and roundness. The major problem with this method is that it can add a subjective element that can affect the result.

Another method that is widely used to characterize the roughness of particles is Fourier analysis [7]. This analysis, which uses a 2D picture of a particle to identify its roughness, is

mainly used in geological research. Much research has been done in different fields to produce mathematical equations for this analysis. Prior to the use of Fourier analysis a major problem was that this method required that the centroid of a particle be accurately identified, a requirement that was particularly difficult to meet when the particle had a complex shape. To overcome this problem, complex Fourier analysis was developed. With this analysis, it is unnecessary to identify the location of the centroid. However, despite this major advantage, Fourier analysis greatly sacrificed the convenience because the mathematical equation developed for this analysis became very complex. This problem of applicability and complexity associated with the methodology is the reason why it has not been more widely used.

3.2 ROUGHNESS FRACTAL DIMENSION, D_R

For this research, fractal analysis was used to measure and quantify particle roughness. In fractal analysis, three different methodologies are generally used to obtain the roughness fractal dimension, D_R: Parallel line method, Area-Perimeter Method with manual digitization and Area-Perimeter with automatic digitization. In this section, the procedures of these three methods are introduced.

3.2.1 Parallel-line method, divider method

Based on the theory that a line that is irregular at any level of scrutiny is fractal and that the length of that line can be defined by mathematical model, Mandelbrot proposed Equation 3-1 [(5)].

$$P(\lambda) = n\lambda^{1-D_R} \tag{3-1}$$

where P(λ) is the measured line length; n is the proportionality constant; and λ is the step length. By taking the logarithm of Equation 3-1, the linear relationship of D_R and linear slope coefficient, m, can be determined as in Equation 3-2.

$$D_R=1–m \tag{3-2}$$

where m is the linear slope coefficient. The process of obtaining this value will be explained later in this section.

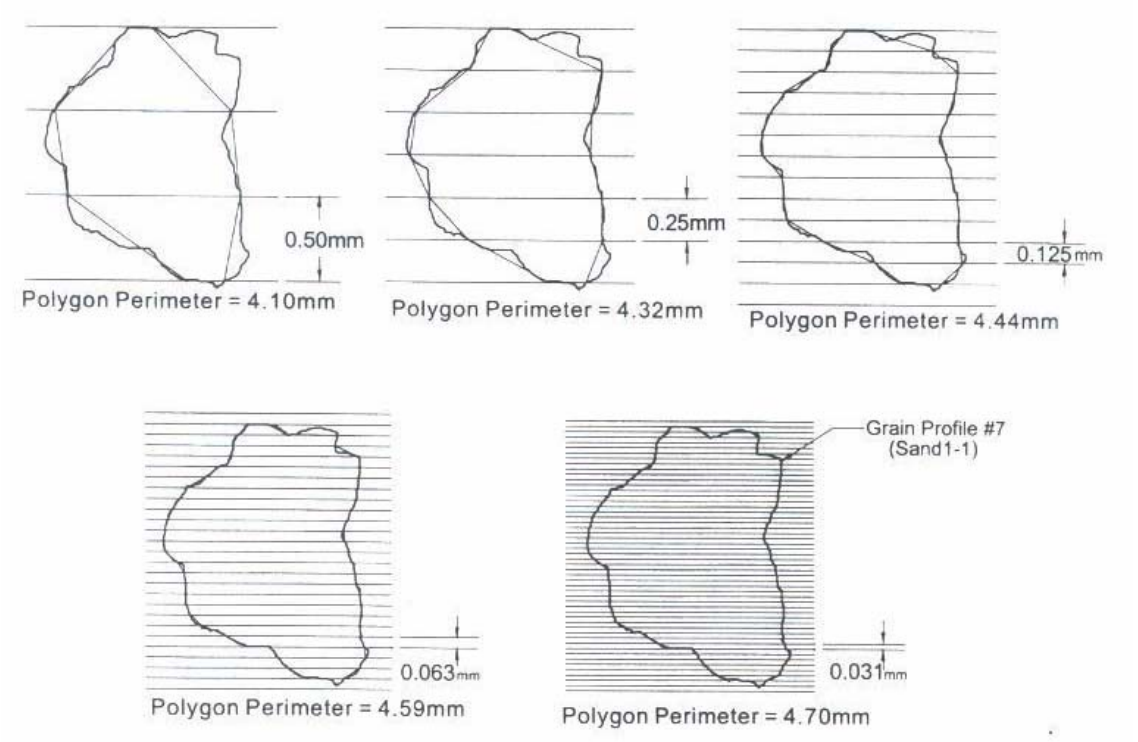

Figure 3.1: Example of parallel-line method with different step length, λ.
(adapted from Hyslip and Vallejo [5])

With the parallel line method, first a set of parallel lines of same distance are laid on top of outlined 2D picture of an object that is being considered. (See Figure 3.1).This outline is called the fractal line. The distance between the parallel lines are called the step length, λ. Next, the length of the straight line connecting intersections of fractal lines and parallel lines are measured. Then this process is continued for the whole perimeter of the object.

As shown in Figure 3.1, as λ gets increasingly smaller, P(λ) increases. The sum of the length of the straight lines measured is the measured line length, P(λ). This P(λ) must be measured with different λs. Then the plot of λ and P(λ) can be prepared as shown in Figure 3.2. As mentioned previously, it can been seen from Figure 3.2 that as λ decreases as P(λ) increases.

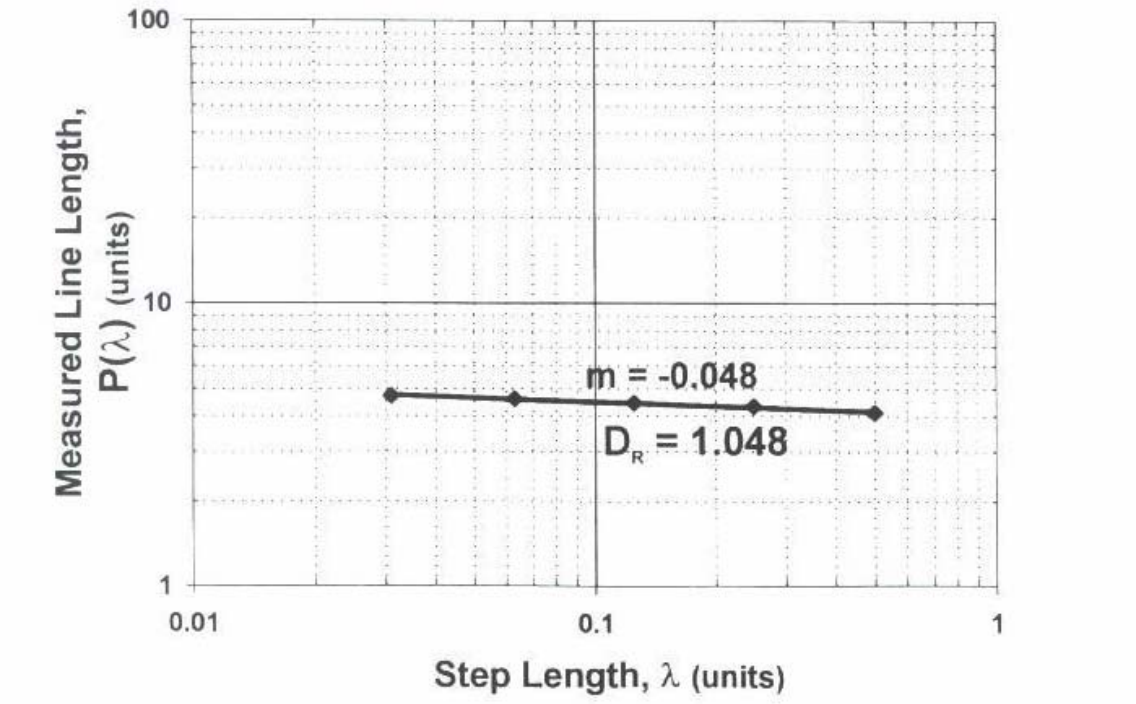

Figure 3.2: Step Length, λ, and measured line length, P(λ).
(adapted from Hyslip and Vallejo [5])

The slope of this line is linear slope coefficient, m, in Equation 3-2. As the fractal line becomes more irregular, the D_R increases. The parallel-line method, like the other two methods, is limited in that it cannot distinguish between structural and textural difference; thus, the D_R obtained in this research is the composite value of both types of roughness. This composite value offers a good quantified measurement of roughness, which is useful.

3.2.2 Area-perimeter method, manual digitization

It can be seen from the equations that any linear extent of geometrical patterns such as length, L, the square-root of area, $A^{1/2}$, or the cube-root of volume, $V^{1/3}$, have constant ratios. For example, the equations for the perimeter and area of a circle are as follows:

$$P=2\pi r \text{ and } A=\pi r^2$$

Taking the ratio of the linear extent of these two values, P and $A^{1/2}$, yields the following relationship,

$$P/A^{1/2}=C_c$$

where C_c is a constant ratio of a circle. For any size circle, the value of C_c is equal to $2\pi^{1/2}$ and this value is independent of the radius of the circle. There are similar ratios for other shapes. For instance, the constant ratio of the linear extent of P and $A^{1/2}$ for square, C_s, is 4.

By using this relationship of linear extent, Mandelbrot suggested that the population of geometry that is similar in fractal shape with in the group can lead to the fractal dimension with quantitative measurement of the roughness of population [5]. Thus, Mandelbrot proposed Equation 3-3 which yields the constant, c, as the ratio of the linear extent of perimeter, P, and area, A. This equation is further derived as Equation 3-4.

$$C=\frac{(\text{perimeter})^{1/D_R}}{\text{area}^{1/2}} \quad (3\text{-}3)$$

$$D_R=2/m \quad (3\text{-}4)$$

Equation 3-4, like Equation 3-2, shows the relationship between slope coefficient, m, and roughness fractal dimension, D_R. The m in Equation 3-4 represents the slope coefficient m, which is different line from m in Equation 3-2. m in Equation 3-4 is the slope coefficient of plot

of the areas and perimeters of multiple particles in a log-log scale. Figure3.3 shows the example plot of the areas and perimeters in log-log scale.

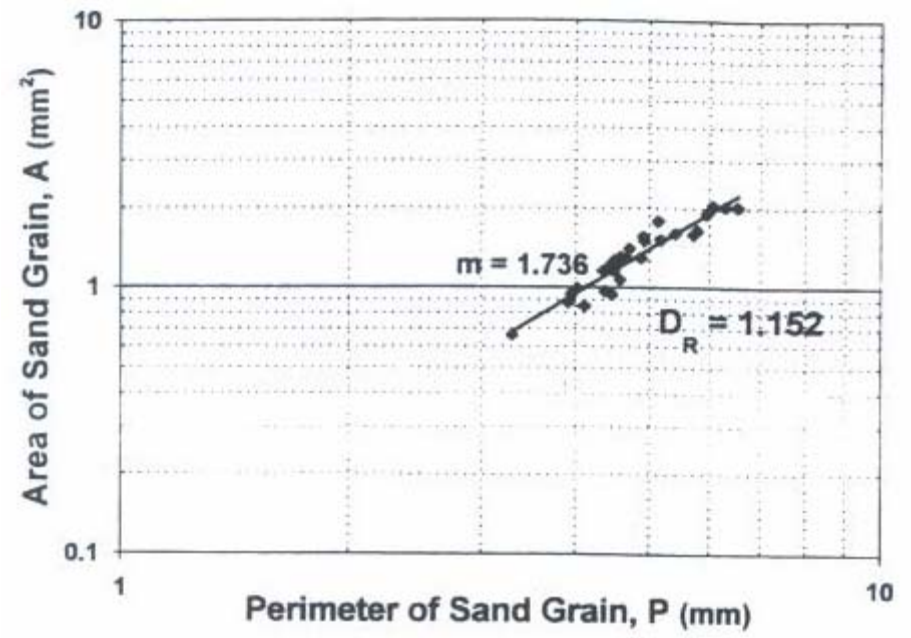

Figure 3.3: Plot of area and perimeter of particles in log-log scale using manual digitization method.
(adapted from Hyslip and Vallejo [5])

The area and perimeter of particles in Figure3.3 was measured by first digitizing the picture of the particles and then utilizing computer software to measure these two values for each particle. The computer software used for this purpose in this research was Image J, with which a picture can be changed from color to black and white. Once the picture has been changed into black and white a particle outline can be generated. Using this outline Image J accurately measures the area and perimeter of the particles.

3.2.3 Area-perimeter method, image analysis system

This area-perimeter method is based on the same theory as manual digitization, which was introduced in previous section. The two methods differ with regard to how the pictures are taken and use of image analysis system. With the image analysis system, pictures are taken with a specially equipped camera that is attached to an image analysis system. The advantage of this method is that it can analyze the pictures easily and quickly than the manual digitization method does.

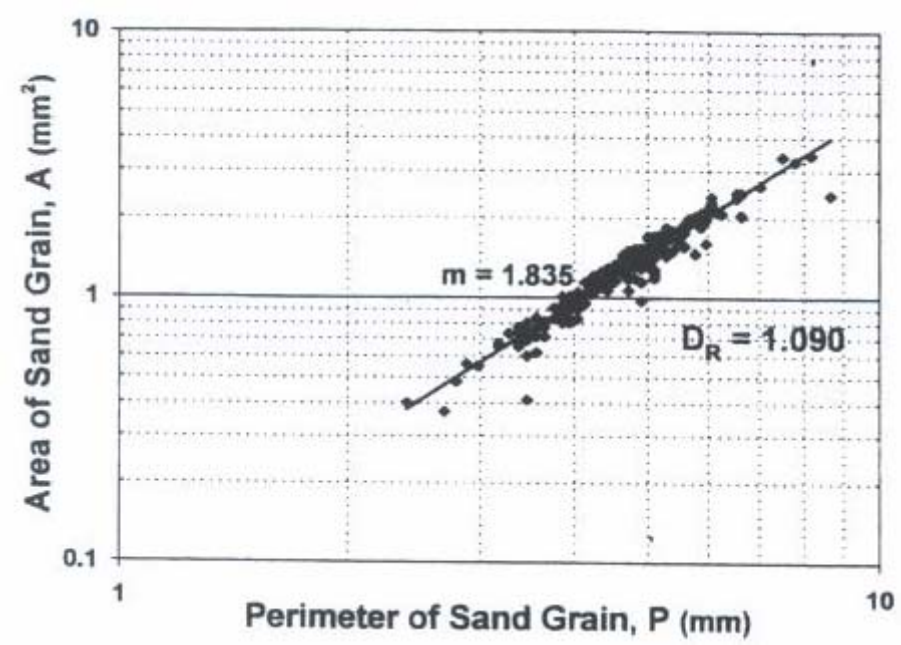

Figure 3.4: Area and perimeter of particles in log-log scale using image analysis system. (adapted from Hyslip and Vallejo [5])

Figure3.4 shows the plot of area and perimeters of particles analyzed by the image analysis system. By comparing the plot in Figure 3.3, the plot of area-perimeter with manual digitations, and the plot in Figure 3.4, it can be seen that the image analysis system has analyzed

considerably more particles. However, the equipment necessary to use for the image analysis system is often not available (and so was not used for the research described in this paper).

3.2.4 Comparison of fractal dimension of particle roughness

Hyslip and Vallejo [5] has developed Figure 3.5, which shows the roughness fractal dimension, $D_{R,}$ of six different types of sand determined using three different methods. In this figure, use of the area-perimeter method using the image analysis system does not have the result of D_R for sand types 2 and 3. The area-perimeter method with image analysis system could not be used for sand types 2 and 3 because the sand size was too small for the camera to take a picture.

By comparing the D_R calculated using two different area-perimeter methods, it can be seen that the D_R calculated produced using the manual digitization method is higher than that produced with the image analysis method for all the comparable sand types except for type 5. As mentioned previously, the image analysis method often uses a lower magnification camera; thus, the pictures of sand type 5 taken using the image analysis method might represent only the structural aspect and disregard the textural roughness. Consequently, the resulting D_R would be lower. The result produced with the parallel-line method has much different characteristics than those produced using the two area-perimeter methods, perhaps because of an important difference in procedure. The parallel-line method calculates a D_R for each particle and then takes the average but the area-perimeter method takes the average of the population of particles and the D_R obtained represents the whole population. From the plot of the D_R in Figure 3.5 obtained by the parallel-line method, it can also be seen that the difference between the results is substantially less than that of the two area-perimeter methods.

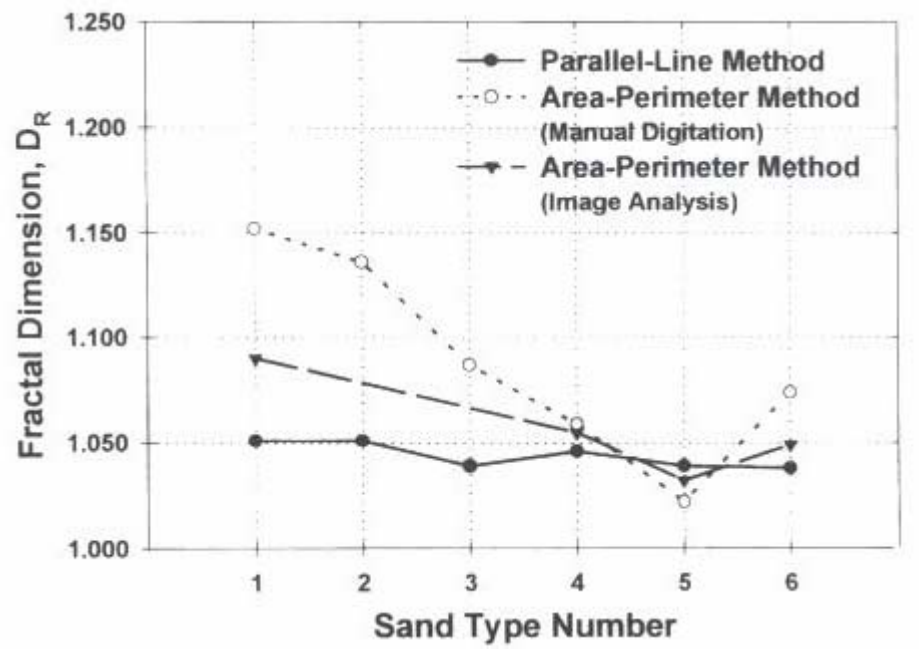

Figure 3.5: Comparison of result from different roughness fractal dimension, D_R.
(adapted from Hyslip and Vallejo [5])

3.3 OTHER SIZE DISTRIBUTION ANALYSIS

The size of particles in soil mass varies greatly. Even in two soil masses that are from the same location, the size distribution of the particles in each would not be the same. In order to classify the soil properly, its specific particle size distribution must be understood. Often, this is presented graphically with a grain size distribution plot.

Based on the plot of a grain size distribution, soil can be classified into specific types. In order to classify the soil from this plot, two major classification systems have been used. The first system is the AASHTO soil classification system which is mainly used to classify highway subgrade materials. Another widely used soil classification system is USCS (Unified Soil Classification System), which is used in practically all geotechnical work. Both of these systems

consider not only the data from grain size distribution plots but also soil properties such as plastic limit, liquid limit and plasticity index, together known as Atterberg limits. Since the purpose of this research is to study the fragmentation of granular material, it is desirable to use the classification system which is solely based on the size distribution of particles. Although, the AASHTO soil classification system and USCS are very useful and widely used, since the property of soil is also considered in both of these classification systems, the resulting classification would not be based purely on the size distribution of particles. Also the results of these two classification systems do not yield numerical values. Thus, another classification system must be considered.

There are two coefficients that represent soil size distribution: the uniformity coefficient, C_u, and the coefficient of curvature, C_z. Following are the equations to determine these two coefficients:

$$C_u = \frac{D_{60}}{D_{10}} \quad \text{and} \quad C_z = \frac{D_{30}^2}{D_{60} * D_{10}}$$

where, D_{10}, D_{30} and D_{60} are diameters which correspond to percent finer of 10%, 30% and 60%, respectively. These diameters can be read from grain size distribution curves. Soil is considered uniform when its uniformity coefficient is less than 2. As can be seen from above equations, these two coefficients consider an insufficient number of points in the grain size distribution curve. Thus, these two coefficients are limited in their ability to accurately represent true size distribution.

3.4 FRAGMENTATION FRACTAL DIMENSION, D_F

Large-scale fragmentation of a rock body is often the result of fragmentation that occurs at any smaller scale. This small-scale fragmentation occurs wherever a weak link in a rock mass exists. Since a weak link could exist anywhere in a rock mass, it can be said that the fragmentation of granular material is irregular and random. Since large-scale fragmentation is the result of this smaller-scale fragmentation, large-scale fragmentation is also irregular and random. Given the characteristics of fragmentation, irregularity and randomness, it can thus be said that the fragmentation of the rock body is fractal. Given the fragments, irregularity, and randomness of both the rock mass and any of the fragments derived from it, it can thus be said that the fragmentation of rock is fractal. Given these characteristics and this relationship, fractal analysis can be used to quantify the size distribution of the granular materials that were tested in this research.

Equation 3-5 was proposed by Tyler and Wheatcraft, who used fractal theory to determine the normalized quantification of the size distribution [5].

$$\frac{M(R < r)}{M_T} = \left(\frac{r}{r_L}\right)^{3-D_F} \tag{3-5}$$

where M(R<r) is the cumulative mass of particles with size R smaller than a given comparative size r; M_T is the total mass of particles; r is the sieve size opening; r_L is the maximum particle size as defined by the largest sieve size opening; D_F is the fragmentation fractal dimension. M_T is used for normalization and r_L is used to bound D_F above zero. Once Equation 3-5 was derived, Equation 3-6 was proposed.

$$D_F = 3 - m \tag{3-6}$$

where m is the slope coefficient that can be determined from the plot of $M(R<r)/M_T$ versus r/r_L in a log-log scale. The advantage of this method is that it can utilize the data of grain size distribution curve just the same as uniformity coefficient and coefficient of curvature. Thus, this method can be used as easily as two other coefficients. Another advantage of this method is that D_F takes into account more points in the grain size distribution curve than two other coefficients. As a result, the value of D_F that is determined can represent a more accurate size distribution. Also, it should be noted that when the value of D_F is small, it indicates that the size distribution is not completely fractal. This most commonly occurs on a sample that hasn't yet been subjected to any stress. At this point, a sample is not yet fractal, in other words, the size distribution of sample is still more uniform than fractal.

3.5 SUMMARY

For this research, the area-perimeter method with manual digitization technique was used to determined roughness of the particles because of its advantage over other two methods. The resulting D_R of the sample determined by parallel-line method fell within a similar range. In addition to this problem, when the parallel-line method is used, the D_R must be calculated separately for each particle, a process that would have been too time-consuming. As mentioned earlier, area-perimeter method using image-analysis system was not an option since the equipment required was not available.

Applying fractal analysis to determine the size distribution of sample is as easy as finding the coefficients of the size distribution of the particles. However, considering the grain size distribution of entire sample will result in a more accurate particle size distribution.

4.0 DIRECT SHEAR TEST

When force is applied to granular material, the force is transmitted through the material via a force chain, which it forms. The importance of a force chain is that when a granular particle is not a part of a force chain, it does not support any loading and so is free from crushing. The purpose of performing a direct shear test in this study was to observe the formation of force chains created under different stress combination and with different samples. By using different combinations of normal and shear stresses, the influence of applied force on the formation of a force chain should be observed. Although it was ideal to study the formation of force chains in 3-dimensionally to simulate the actual situation, the force chain formation studied in this experiment was only 2-dimensional since the direct shear test was 2 dimensional. Nonetheless, the test results obtained provided a good simulation of the actual formation of a force chain. The figures obtained using the discrete-element method, or DEM, will be used for comparison purposes. DEM is a numerical model used to describe the mechanical behavior of the discs or spheres and was originally developed by P.A. Cundall and O.L Strack [(8)].

4.1 EQUIPMENT AND MATERIAL

The direct shear device used in this test is shown in Figure 4.1. This device can apply both normal and shear stress to the sample placed in the square box placed in the bottom right-hand corner of Figure 4.1. This square box has dimensions of 7.5 cm in height and width by 3.0 cm in depth. This square box consists of two parts, upper and lower. The upper part can be moved downward or toward the left by applying normal and shear force, respectively. The bottom part is fixed. Two of the four gauges shown in this figure read the normal and shear ring deformations caused by the applied loading. From right to left, the four gauges are as follows; the first gauge measures the shear ring deformation, the second gauge measures the vertical deformation, the third gauge measures the normal ring shear deformation, and the fourth gauge measures the horizontal deformation. By measuring the ring deformation and utilizing the calibration chart, the applied force can be determined. Then, dividing this force by the area of the cross section of the sample yields amount of stress applied to the sample. The other two gauges measure the displacement of the upper part of the box due to normal and shear stresses.

The material that was tested in this experiment was two different sets of short wooden sticks, each of which has a length of 3.0 cm the same as the depth of the square box. The wooden sticks in the first set were all cylindrical shape and had same size and the wooden sticks in the second set were different shapes and sizes. First set of sticks were used to simulate the formation of force chains in an ideal situation. The second set of sticks simulated the actual formation of a force chain in granular material.

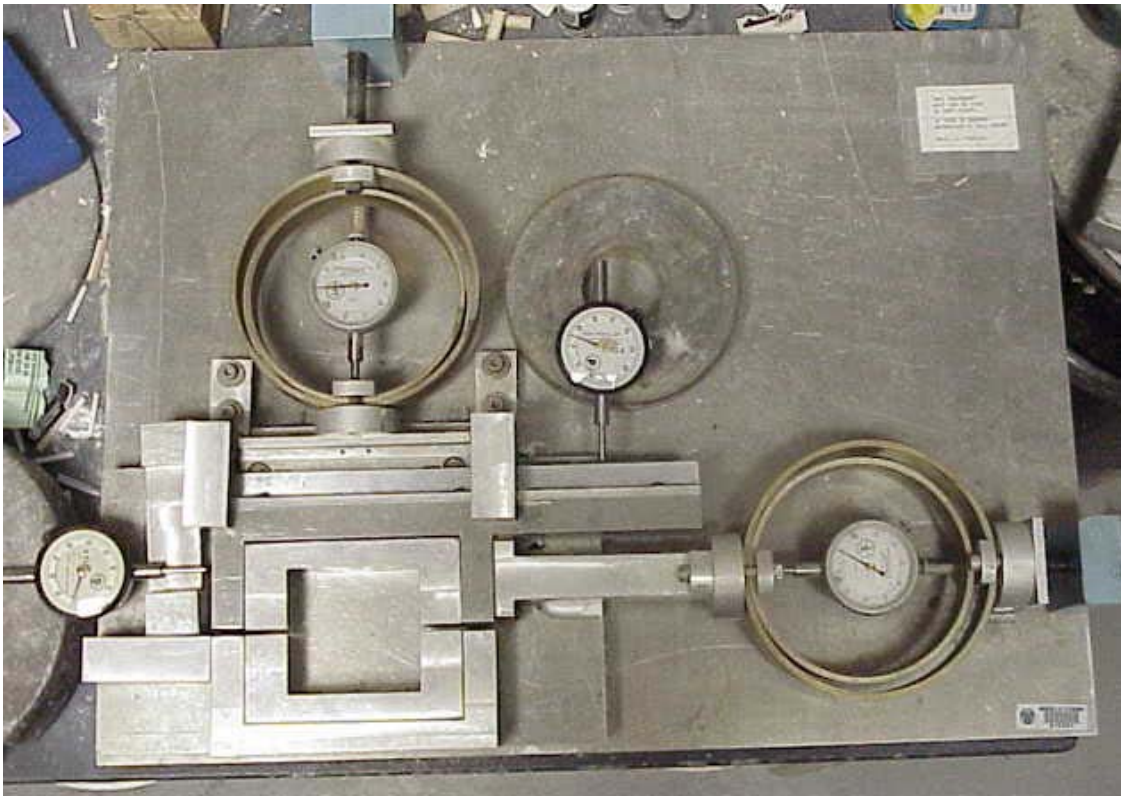

Figure 4.1: Direct shear device used in this test.

4.2 RESULT

4.2.1 First Set

4.2.1.1 Normal Load The first set of wooden sticks, cylindrical and all the same size, were tested under two different combinations of normal and shear stress. The first combination was 57.33 kPa of normal stress and no shear stress. Vertical deformation was $1.3*10^{-4}$ m and there was no horizontal deformation. Figure 4.2 shows the original structure of the sticks, and Figure 4.3 shows the new structure formed after stress was applied to the sample. In Figure 4.3, sticks that were loose, i.e., sticks that were not taking any loading, were removed. By comparing these

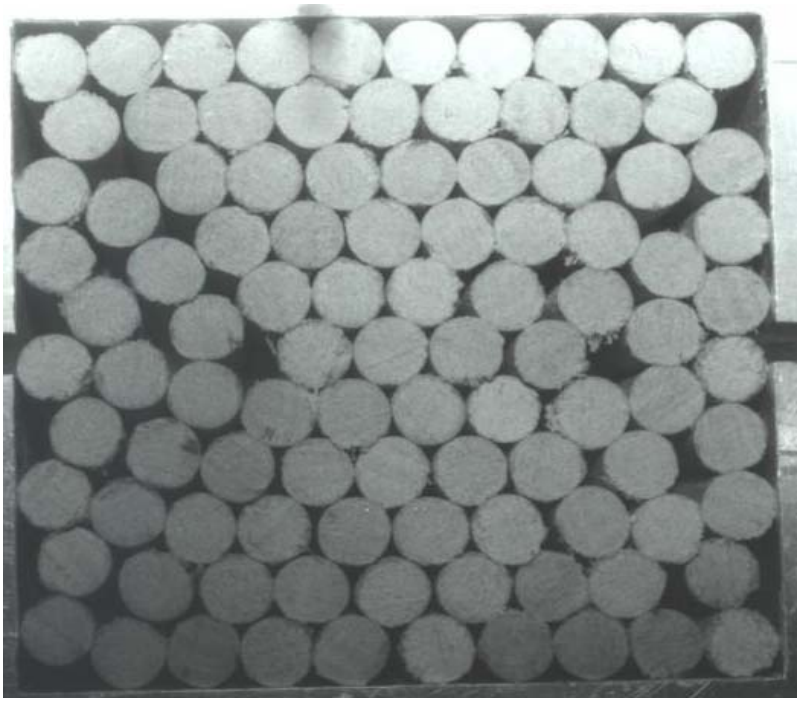

Figure 4.2: Structure of sticks before applying 57.33 kPa normal stress.

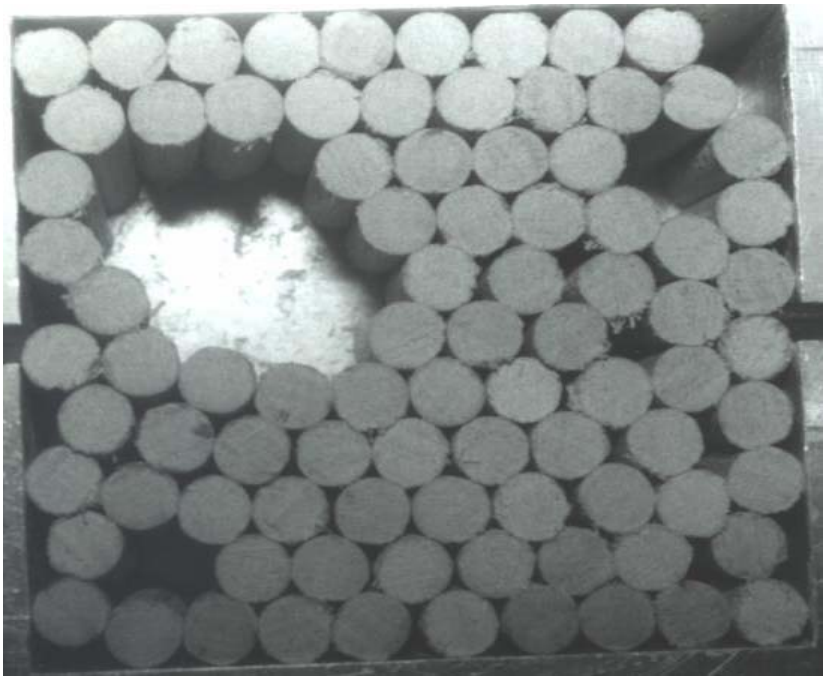

Figure 4.3: Structure of sticks after applying 57.33 kPa normal stress.

two figures, it can easily be seen that after loading was applied, a cluster of sticks in one section was not taking any loading. This suggests that a force chain was not formed in this specific area. Since the force chain caused the sticks to create an arch, the sticks under this arch didn't have loading transferred to them; all the force was transferred to both end of arch. In Figure 4.2, it can be seen that there were many spaces between sticks in the area where the arch was later formed in Figure 4.3. This relatively large space between the sticks before stress was applied, could have prevented these sticks from taking any loading. Since the deformation caused by this combination was small, sticks that were loose at the original state remained loose. To confirm this result, there were two other sticks that were not taking any loading, one at the top right-hand corner and another one at the bottom left-hand corner. These two sticks also had relatively large spaces surrounding them before the test.

4.2.1.2 Normal and shear Load The second combination of loading applied was 57.33 kPa of normal stress and 79.11 kPa of shear stress. The horizontal deformation was measured as much greater than the vertical deformation: the vertical and horizontal deformation was measured as $5.6*10^{-4}$ m and $3.43*10^{-4}$ m, respectively. When shear stress was applied, the upper part of the box moved toward the left, and the sticks were able to move to the left. The new space for the sticks to move to was created relatively easily by horizontal deformation compared to vertical deformation. On the other hand, in order to cause vertical deformation, sticks also required spaces to move into, but since there was not much space in the original structure, the sticks were stuck in the original positions so the vertical deformation was much less. Although the amount of normal stress applied to the sample was same, the vertical deformation that occurred in this sample was grater than the vertical deformation that had occurred in the first combination of

stresses. This was because the second combination of stresses allowed sticks to move more by horizontal deformation than the first combination. Consequently, more space was created for sticks to move around.

Figure 4.4 and 4.6 contain pictures showing the structures before and after the stress was applied, respectively. There was a huge arch created in the bottom right-hand corner in Figure 4.6. This result indicates there was no force transferred to this area. The arch created by the application of shear stress in this area was much greater than the arch created by normal stress in the previous test. Since the upper half of the sticks were moving toward the left as normal stress was applied at same time, the resulting force was transferred diagonally toward the bottom left corner through the sticks. Figure 4.5 is the picture of the particles simulated by DEM [(9)]. In this picture there was no stress applied to the particles and shows the position of the particles if no stress had been applied. Figure 4.7 is the picture of the same sample after normal and shear stress was applied. The black lines in this picture represent force chains formed by applied stress. The thickness of the line represents the intensity of the force chain: a thick line means the force being transferred is greater than a thinner line.

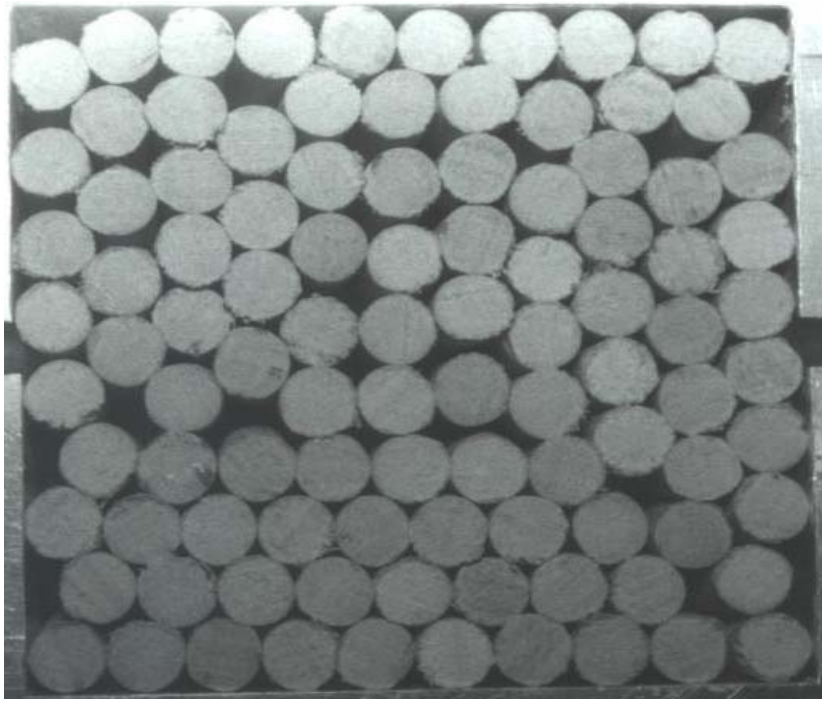

Figure 4.4: Structure of sample with cylindrical sticks before applying 57.33 kPa of normal stress and 79.11 kPa of shear stress.

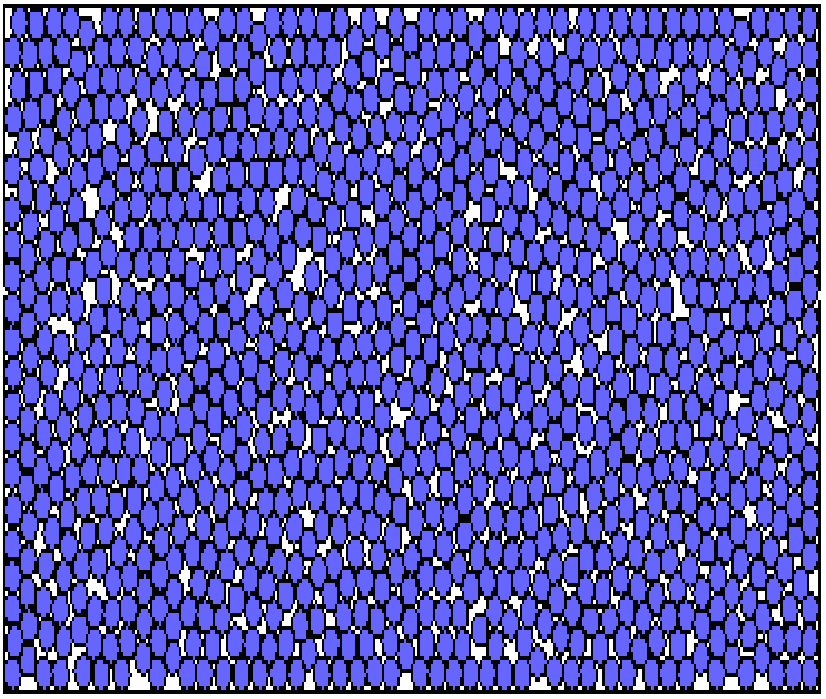

Figure 4.5: Structure of particles from DEM.
(adapted from Lobo-guerrero and Vallejo [9])

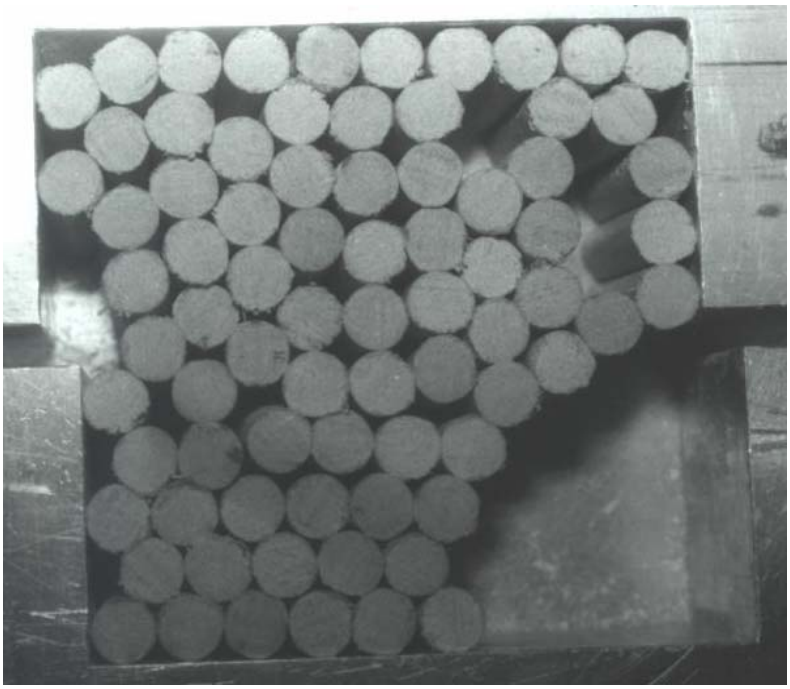

Figure 4.6: Structure of sample with cylindrical sticks after applying 57.33 kPa of normal stress and 79.11 kPa of shear stress.

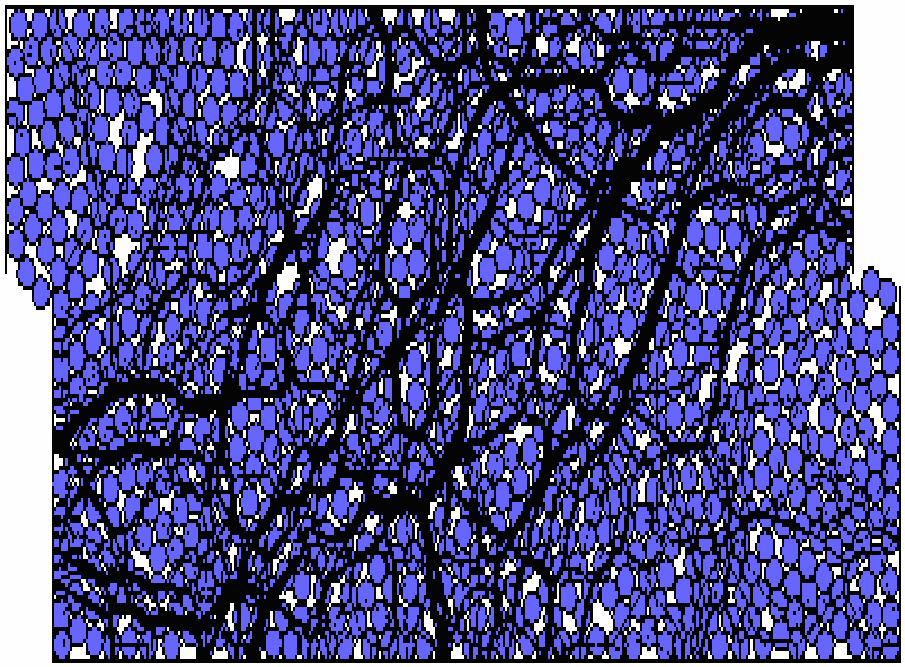

Figure 4.7: Structure of particles and formation of force chain under normal and shear stress produced by DEM.
(adapted from Lobo-guerrero and Vallejo [9])

4.2.2 Second Set

4.2.2.1 Normal Load The second sample of sticks had various shapes and sizes so that the resulting formation of force chain would more closely resemble the situation of actual granular material than with the first sample of sticks, which was used as to simulate an idealized situation. The following figures, Figures 4.8, 4.9, 4.10, and 4.11, are pictures showing the structure before and after two different normal stresses were applied. Figure 4.8 and 4.9 are the before and after pictures of 57.33 kPa of normal stress being applied, respectively. And Figure 4.10 and 4.11 are the before and after pictures 114.67 kPa of normal stress being applied, respectively. As can be seen from Figure 4.8 and 4.10, sticks were packed randomly in both cases and the density of packing was also similar. However, these two different normal stresses yielded very different results. Figure 4.9 shows that with under 57.33 kPa of normal stress, there were many sticks that were not part of the force chain formed by the applied stress. On the other hand, Figure 4.11 shows that all the sticks were taking some loadings when 114.67 kPa of normal stress was applied. This result indicates that the greater number of force chains was formed by increasing normal stress. Figure 4.12 shows the formation of force chain under high normal force produced by DEM. In this figure, it can be seen that force chains were formed through out the particles. Some particles were part of lower intensity than other, but they were still part of smaller intensity force chain. When normal stress of 57.33 kPa was applied, arches were created at several different areas, but when normal stress was increased to 114.67 kPa, these arches disappeared. This could be because of the different amount of deformation caused by these two loadings. When normal stress was increased from 57.33 kPa to 114.67 kPa, the vertical deformation increased from $2.5*10^{-4}$ m to $2.4*10^{-3}$ m. Thus, when normal stress of 114.67 kPa was applied, it

created the contacts between sticks forming the arch and the sticks under the arch so force started to transfer to the sticks under the arch, which might have remained loose under normal stress of 57.33 kPa.

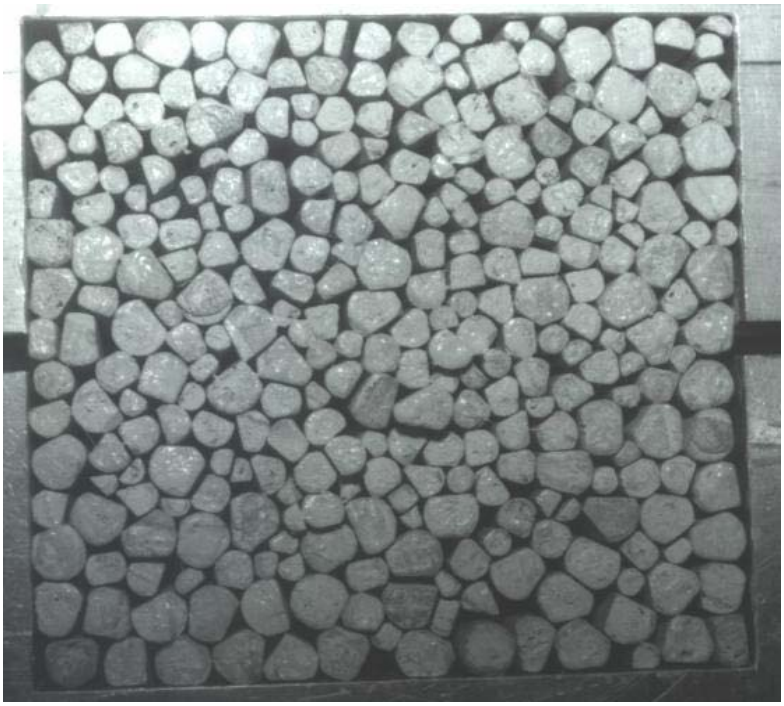

Figure 4.8: Structure of sample with various types of sticks before applying 57.33 kPa of normal stress.

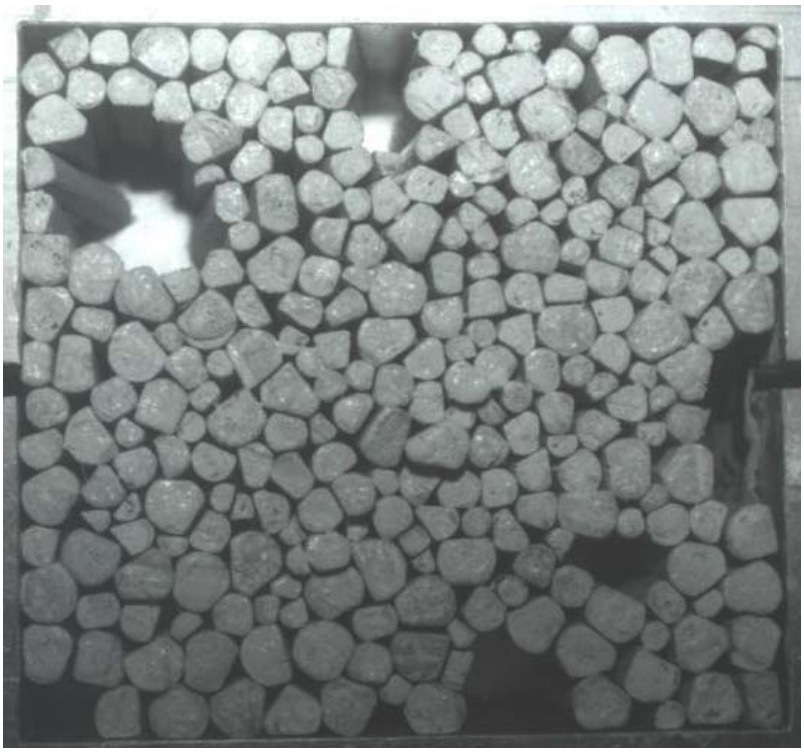

Figure 4.9: Structure of sample with various types of sticks after applying 57.33 kPa of normal stress.

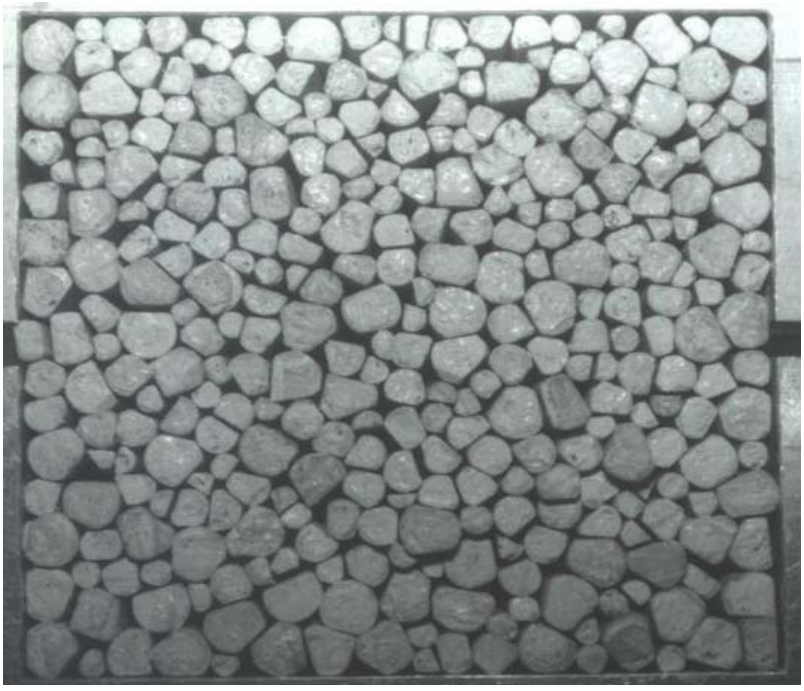

Figure 4.10: Structure of sample with various types of sticks before applying 114.67 kPa of normal stress.

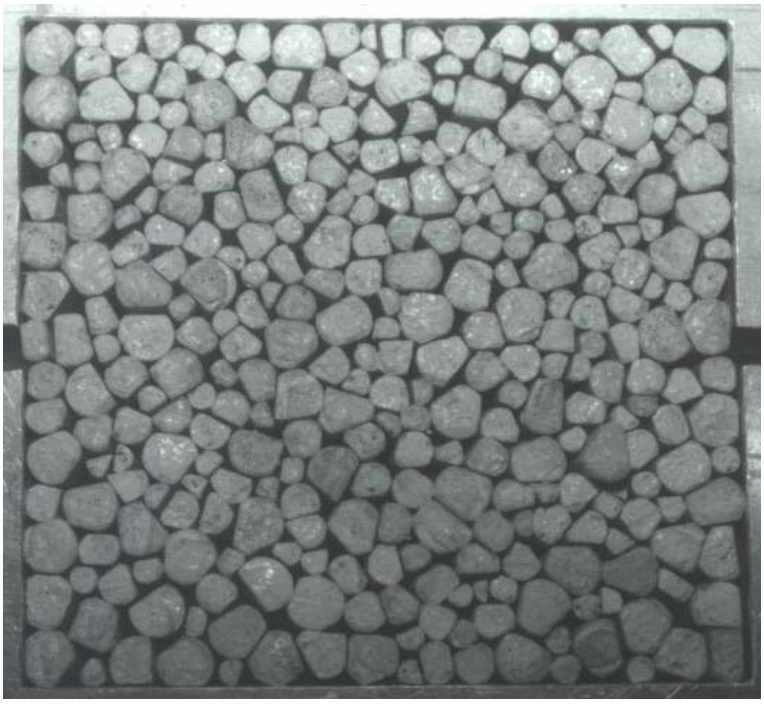

Figure 4.11: Structure of sample with various types of sticks after applying 114.67 kPa of normal stress.

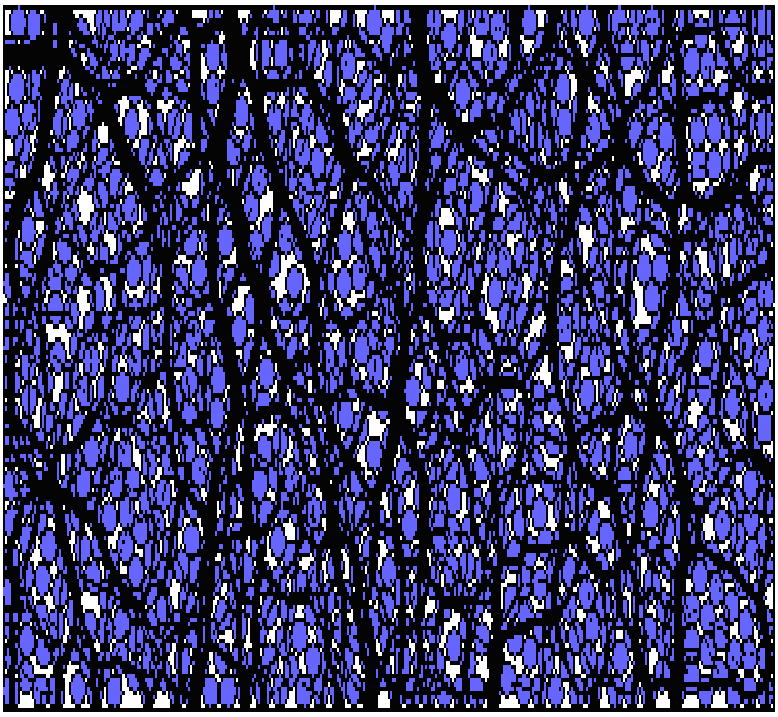

Figure 4.12: Structure of particles and formation of force chain under normal stressproduced by DEM.
(adapted from Lobo-guerrero and Vallejo [9])

4.2.2.2 Normal and shear Load The following three figures are pictures of structures resulting from three different combinations of normal and shear stresses. Figure 4.13 shows the resulting structure of 57.33 kPa and 79.11 kPa of normal and shear stress, respectively. This combination is the same as that applied to the sample with cylindrical sticks earlier. Consequently, not only were the resulting force chains similar to those obtained using cylindrical sticks, but the vertical and horizontal deformations were similar as well. The vertical deformation was $1.19*10^{-3}$ m and horizontal deformation was $3.05*10^{-3}$ m. There was a large arch produced in the bottom right-hand corner and some other sticks were loose. However, some differences can be observed between these 2 sets of results, too. In this test, where the force chain formed reached the corner of bottom right-hand corner, the result differs from that obtained using cylindrical sticks. From this direct shear test, the intensity of the force chain cannot be determined. Thus, this force chain reaching to bottom right-hand corner might be under a small amount of force caused by vertical loading. The number of sticks used in this test was much greater than the number of cylindrical sticks, so the formation of a force chain might have become more complex and some force was transferred to the bottom right corner. Figure 4.7, shows that some force chains with small intensities were formed to the bottom right hand corner as well. Thus, from the result of the experiment and from DEM simulation, it could be concluded that when there are many small particles a force chain can be formed toward the bottom-right hand corner while the majority of the force chains are formed diagonally through the sample from top right-hand corner to bottom-left hand corner. Thus, such a force chain was not formed in the sample with cylindrical sticks, which sticks were much larger than this sample or simulated particles in DEM, when under the same combination of stresses.

Figure 4.14 is a picture of a sample containing various types of sticks under normal and shear stress of 114.67 kPa and 98.87 kPa, respectively. Compared to the previous test with the same sample, normal stress was doubled, and the shear stress was increased by 19.76 kPa, or about 30%. Vertical and horizontal deformations occurred after the normal and shear stresses applied were $1.57*10^{-3}$ m and $3.76*10^{-3}$ m, respectively. Thus, both the vertical and horizontal deformations were little greater than with the previous test. The only loose sticks in this test were located under the arch of the bottom right-hand corner, which occurred in same location as the previous test, and there were no other loose sticks. The result of this test and the result of the previous test suggest that when shear stress is applied, the increase in normal stress has less influence than the shear stress in both the deformation and the number of loose sticks that are not taking any loading.

Figure 4.15 is a picture of sticks under normal and shear stresses of 171.99 kPa and 131.80 kPa, respectively. The most distinctive characteristic of this picture, as compared to Figure 4.13 and 4.14, is that there was no large arch formed in the bottom right-hand area. Although both normal and shear stress was applied, unlike the previous two tests, no large arch was created. There was small arch formed at this location, but it was much smaller than either of the arches formed in the previous two tests. The reason for this would be that the normal load was too large for a large arch to be created. Just as in the test with 114.67 kPa, there was contact between the sticks forming the arch and sticks under the arch. However, there were some loose sticks and formed small arches in the upper left area. From these two phenomena, it could still be said that when shear stress is applied, the majority of the force chain forms diagonally from the upper right to the lower left. Also it must be noted that the vertical deformation of this test was

only $5.6*10^{-4}$ m and horizontal deformation was $4.32*10^{-3}$ m. The vertical deformation was relatively small compared to the other two tests but the large horizontal movement could have

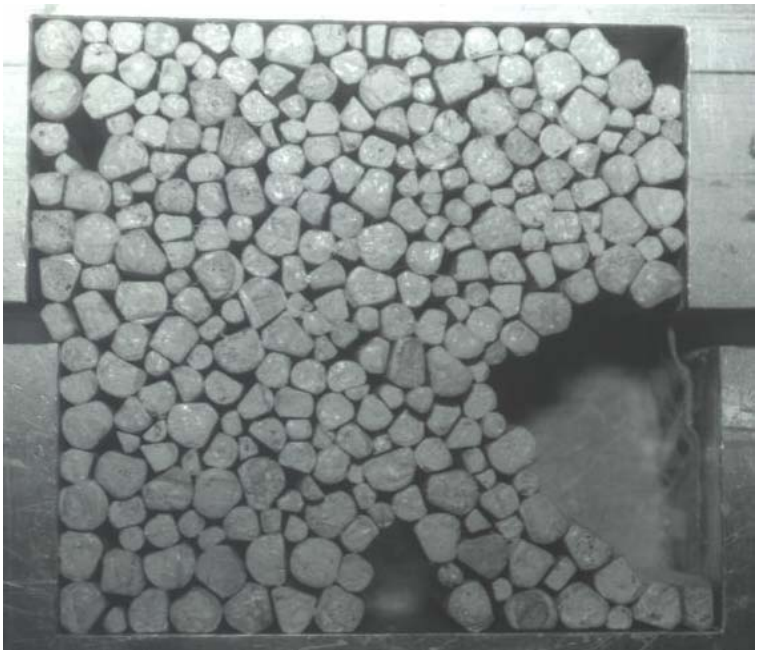

Figure 4.13: Structure of sample with various types of sticks after applying 57.33 kPa of normal stress and 79.11 kPa of shear stress.

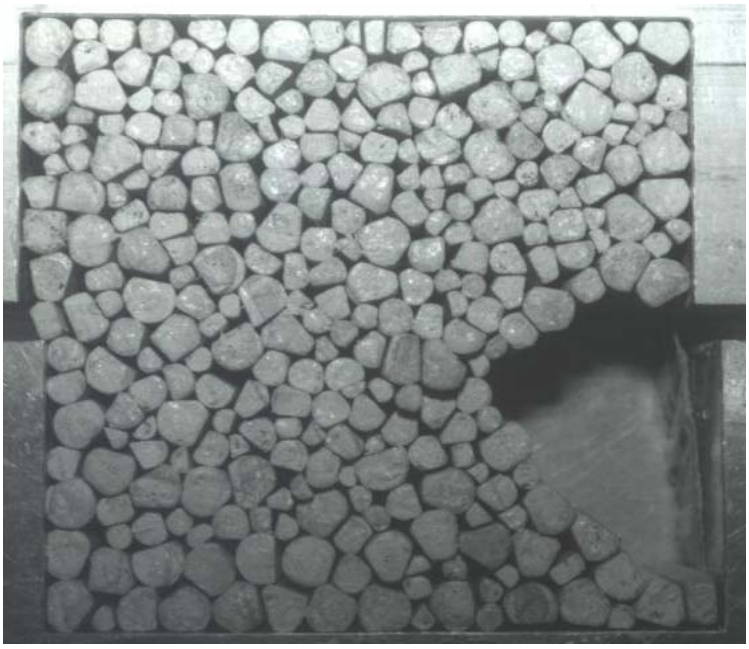

Figure 4.14: Structure of sample with various types of sticks after applying 114.67 kPa of normal stress and 98.87 kPa of shear stress.

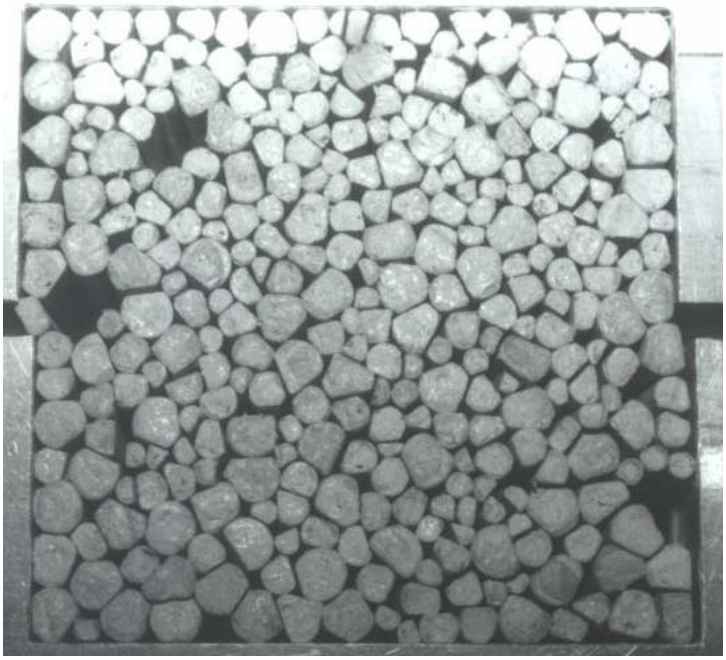

Figure 4.15: Structure of sample with various types of sticks after applying 171.99 kPa of normal stress and 131.8 kPa of shear stress.

caused this small change in vertical deformation. Some sticks in the upper half moved on top of other sticks due to the large degree of horizontal movement, and this could have decreased the overall vertical deformation.

4.3 SUMMARY

In conclusion the formation of force chains was influenced not only by the magnitude of the applied stress but also by the type of stress. In both the idealized situation, simulated using cylindrical sticks, and the actual situation, simulated with various types of sticks, a similar phenomenon was observed. When the sticks were only under normal stress, an arch formed on

top of the place where the lose sticks were originally located. When the sticks were loose, strong contact could not be established, so the force chain could not be formed downward and so instead spread sideways. When both normal stress and shear stress were applied, a large arch was formed in the bottom right-hand area. However, when the large stresses were applied, this large arch did not form because contacts were established between the sticks forming the arch and the other sticks.

By comparing the results of performed test and the DEM, it was found that when normal and shear stress were applied, the majority of force chains formed were from the top right-hand corner to the bottom left-hand corner. Also from this comparison, it could be concluded that when the large number of sticks or particles were used, a force chain with small intensity formed toward the bottom right-hand corner.

It was found that both the vertical and horizontal deformation increased as applied stresses increased. But it was also found that when the large amount of shear stress was applied, the vertical deformation was small despite the large normal stress.

5.0 POINT LOAD TEST

In the history of geotechnical engineering and geology, various types of tests were invented and conducted to determine the strength of rocks. But time has shown that each type of test has its advantages and disadvantages. For example, the triaxial compression test can determine the various properties of samples such as friction angle and cohesion, but this test is time consuming, complicated, and expensive. On the other hand, uniaxial compression test doesn't require a significant amount of time and is much cheaper than the triaxial compression test. But the disadvantage of this test is it requires sample preparation prior to testing. In this research, the point load test was used to determine the strength of rock. The point load test has a couple of strong advantages over other tests. First of all, its sample preparation requirement is minimum compared to other tests. For the point load test, test samples don't have to have the same shape and size. Second, the force that is needed to determine sample strength is much less. Thus it can be done easily. This test also doesn't require much time to perform each test, thus multiple samples can be tested in a short period of time.

The roughness fractal dimension, D_R, of the samples was also determined to make further study of the influence of fragmentation behavior on particle roughness.

5.1 EQUIPMENT AND MATERIAL

The equipment necessary to perform the point load test is the point load testing device, shown in Figure 5.1. This device has two cone-shaped platens, between which the sample is placed. Stress is applied by pumping the lever and the machine's stress gauge reads the stress applied to the supporting platform under the cone. When this test was conducted, the plastic cover was placed so that all the fragmented particles could be collected after the test.

Figure 5.1: Point Load Testing Device.

5.2 PROCEDURE

The purpose of the point load test was to determine the strength of the granular sample that was used in this research and to understand how water content affects the strength of particles. It is well known that the failure of granular material is the result of tensile stress applied to the particle exceeds its tensile strength. In other words, failure of granular material is due to tensile failure. Thus, the strength of granular material can be calculated from the maximum stress applied to the sample or the magnitude of applied stress at the failure.

Before performing the point load test, necessary data must be collected. The stress gauge attached to the point load testing device measures the stress that is applied to the support under the cone platen that had contact with the sample. The area of this supporting platform is $1.4426*10^{-3}$ m^2. Thus, from this area and the stress reading from the gauge, the force that was applied to the sample can be calculated. Since the force reading is from the time of failure of the sample, this force shell be called critical force, F_C. Also prior to the test, three diameters of samples were measured, and then the average of three diameters, d_{avg}, was calculated. The square of this d_{avg} was used as an area of failure surface of the particle. Dividing F_C by d_{avg}^2, the point load strength, I_s, was then calculated. From this theory the following three equations were derived:

$$F_c = \frac{\text{stress reading at the time of failure}}{\text{Area of support}} \quad (5\text{-}1)$$

$$d_{avg} = (d_1 + d_2 + d_3)/3 \quad (5\text{-}2)$$

$$I_s = F_c / d_{avg}^{\,2} \quad (5\text{-}3)$$

Point load tests were performed for both dry and wet granular materials. In each case, 20 samples were tested. According to Oakland and Lovell [10], 20 samples are the minimum number that should be tested in order for the resulting point load strength, $I_{s,}$ to have any statistical meaning. Wet samples were soaked in water for 4 days to make sure they were saturated.

5.3 RESULT

When the point load was applied to each particle, a slight decrease in stress was observed in the stress gauge in the initial stage of test. This phenomenon appeared for every particle that was tested. This decrease in stress was due to the failure of a small portion of the particle that was in contact with the point of the cone. This failure couldn't be considered as a total failure of the particle because this regional failure occurred only on a small portion of particle. Also this failure doesn't propagate through the body; rather it just happens on the surface of the particle. This regional failure can be categorized as either Type 1 or Type 2 failure. Thus, after this regional failure occurs once, the stress increases again until it reaches a particle's maximum strength. At this point, total failure occurs. Unlike the regional failure that occurs during the process, this total failure splits the particle body into 2 or more pieces. When the particle splits into two pieces, failure occurs in the plane between two contact points via a point load device. Since force was applied through the particle by two points, one in the top and one in the bottom, the plane connecting these two points was the plane that is under the most tensile stress. Thus, the plane between these two points was most likely to fail before any other planes.

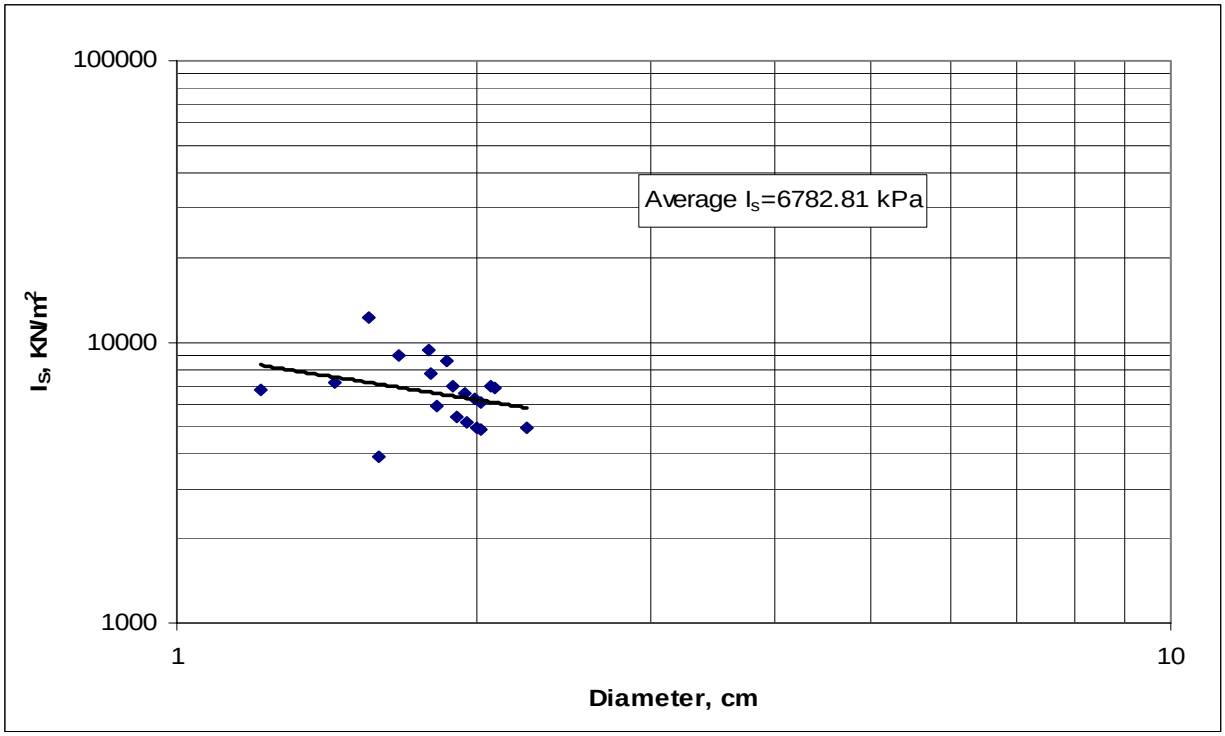

Figure 5.2: Plot of average diameter, $d_{avg,}$ vs. the point load strength, I_s, of 20 dry samples.

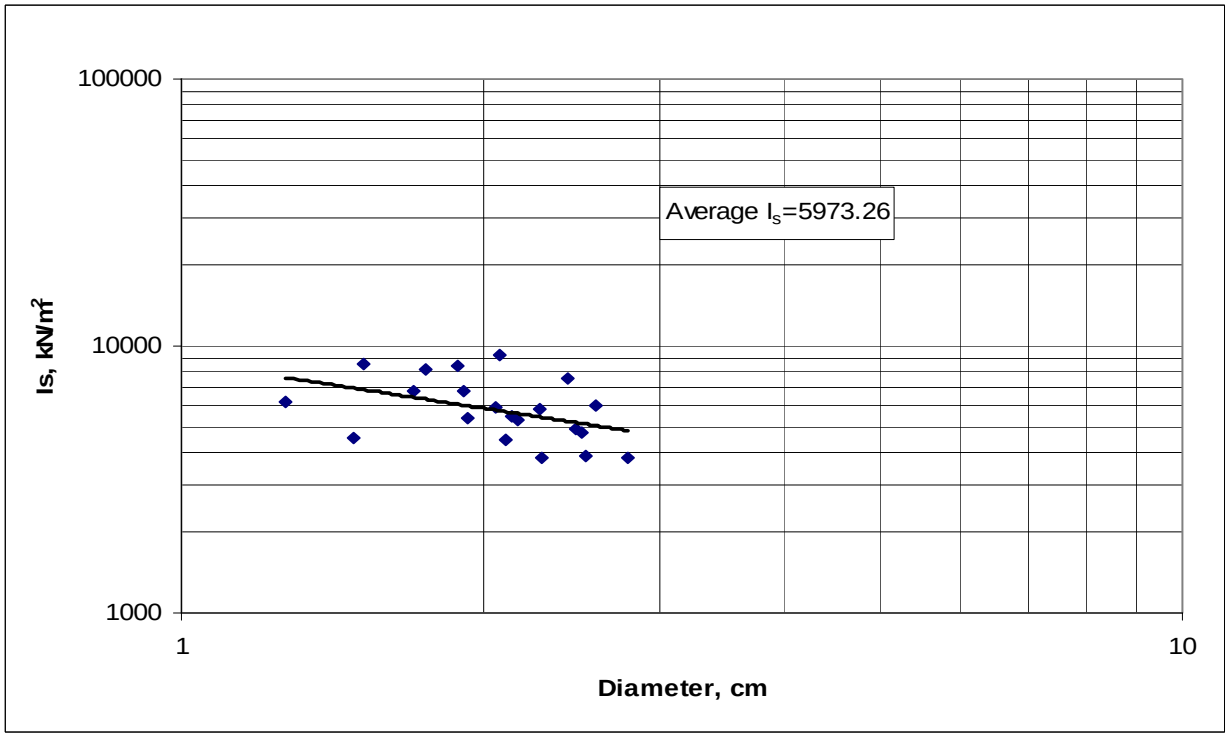

Figure 5.3: Plot of average diameter, $d_{avg,}$ vs. point load strength, I_s, of 20 wet samples.

From the result of the point load test, the average I_s for dry and wet samples was found to be 6782.81 kPa and 5973.26 kPa, respectively. The average I_s for dry samples was found to be about 14% greater than the average I_s for wet samples. I_s was plotted against the average diameter, d_{avg}, of 3 dimensions of corresponding samples, measured prior to the test, to find any correlation between these two parameters. Figure 5.2 is the plot showing the strength of the dry samples and Figure 5.3 is the plot of the wet samples. From the plot, it is discovered that the strength of the material decreases its diameter increases. This trend is observed for both the dry and wet samples.

5.4 DISCUSSION

The result of the point load test revealed many phenomena that must be explained. For example, the result shows that the average I_s of dry samples were greater than that of wet samples. This phenomenon was also studied by many researchers [11, 12, 13, 14]. Hawkins and McConnell [11], who studied the strength of 35 different types of granular materials in dry and saturated conditions. In their result, they found a decrease in strength for 34 types of materials when they were saturated. The percentage of reduction ranged from 5% to 60%. This reduction in strength could be due to stress corrosion or softening of the cementing material. Hawkins and McConnell also concluded that this wide range of reduction in strength is due to the different mineralogy of material.

West [12] proposed another reason for the reduction of strength in the saturated state. From the test result he obtained, he determined different degrees of suction caused by variations in the relative humidity. He found that the strength of granular material that was immersed in

water and achieve a complete saturation had no suction. He also founds that when there was no suction, the strength of granular material was minimal. And as the relative humidity of surrounding the granular material decreases, the strength started to increase gradually. Maximum suction was achieved when the material was dry. However, even if material is considered dry, it is known that there are small amounts of water kept in the pores of the material by capillarity. This water cannot be removed by gravity and can only be removed by heating granular material such as placing in an oven. Thus, Graham West stated that maximum suction occurs in granular material when the relative humidity surrounding the granular material is 0%. At this point, the water content is the lowest possible amount and a great degree of suction is generated.

From the plot of I_s and diameter, it was found that the I_s decreases as the diameter increases. This phenomenon was observed with both dry and wet samples. As discussed in the previous chapter, in order to explain this phenomenon, micromechanics of granular material must be considered. Since the granular materials are created by nature, their properties are not uniform. In other words, granular material has a defect or tiny cracks called flaws within its body. The failure plane propagates through this flaw. Thus, the fewer flaws there are in the body of granular material, the less likely it is that a failure plane will propagate through the body of material. Thus, as the diameter of a particle decreases, the chance a flaw in the body of the particle decreases and, consequently, the strength of the particle increases. Also, as mentioned previously, small particles are often caused by fragmentation of larger particles, and when a larger particle is fragmented, this fragmentation occurs through the flaws in its body. Thus, as a particle gets smaller, there is less chance of its having a flaw in its body.

Studying the relationship between the strength and size of particles, J. Billam [(14)] has found a similar phenomenon. But he has also tested chalk samples to see if there were similar

trends in the relationship between these two parameters, strength and size with that material. He found that the strength of the chalk was always the same regardless of the size of the chalk. This is because flaws are not present randomly in the body of chalk, but have a system of very regular structural flaws which control their behavior.

5.5 ROUGHNESS FRACTAL DIMENSION, D_R

For the sample particles that were tested in the point load test, the roughness fractal dimension, D_R, was also calculated. By studying the change in roughness of sample particles, it became possible to study how the total failure of particles caused by tensile failure effect the roughness of the particles. Figure 5.4 shows the D_R of the samples before the test and Figure 5.5 shows the D_R of the samples after the test. In Figure 5.5 it appears that more particles were considered, but this was only because particles were split into 2 or more pieces after the tests and all the split particles were subsequently taken in account to calculate D_R more accurately.

It can be seen from Figure 5.4, that the D_R of all of the sample particles before the test was found to be 1.0935, and from Figure 5.5, that the D_R of all of the sample particles after the test was found to be 0.9886. This result indicates that samples became smoother after the point load test. Since the only factor that was changed before and after the test was the creation of the failure plane during the test, it can be concluded that the roughness of the failure plane created was less than that of the existing surface. From a visual comparison of the existing surface and failure surface, it was evident that the failure surface had a smoother surface both structurally and texturally.

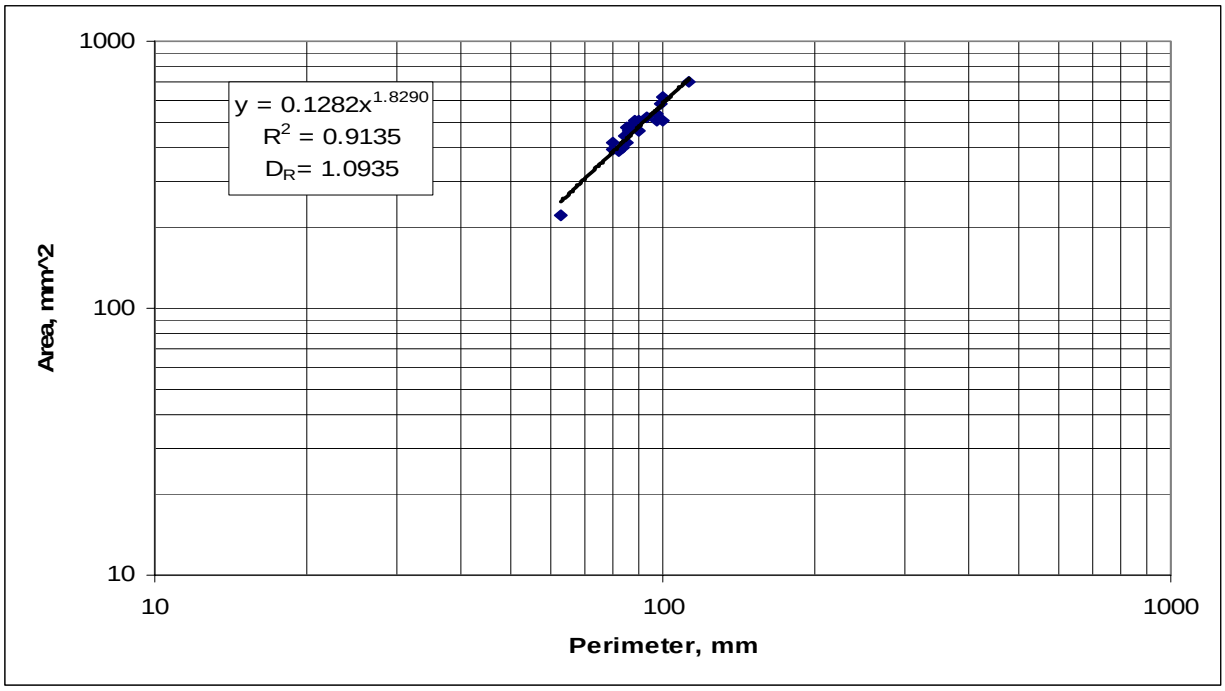

Figure 5.4: Plot of area versus perimeter of sample before the test.

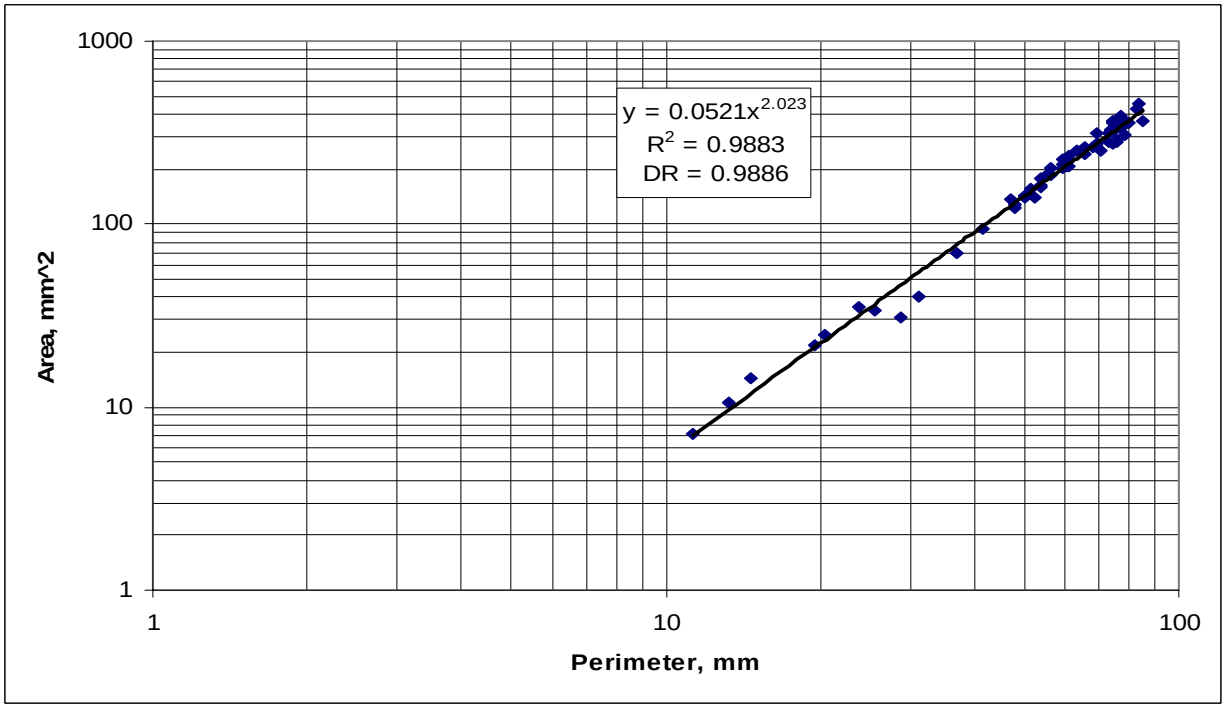

Figure 5.5: Plot of area versus perimeter of sample after the test.

5.6 SUMMARY

The point load strength, I_s, found in this test had two distinctive characteristics. The first characteristic was that the strength of granular material decreased as the diameter of the particle increased. This was caused by flaws that existed in the body of the granular material. The failure plane propagated through these flaws. As the particle's diameter decreased, the chance of its having flaws also decreased and strength of the granular material increased. The second characteristic was that the strength of dry granular materials was greater than the strength of wet materials. There are two factors that can explain this reduction of strength. First, the mineral cements sand particles together, softens when it is saturated. The second reason has to do with the influence of suction: it was found that when granular material is saturated, the water creates no suction. But as the amount of water in the granular material decreases, the suction of the water starts to increase. And when the moisture content is at the minimum, but not zero, the achieved strength of the material is the greatest. Thus, the strength of the material determined in this test could be increased when the relative humidity around the granular material decreased.

Another parameter that was determined by the point load test was the roughness fractal dimension, D_R. Compared to before the test, the D_R decreased after the test. The failure surface created by the total failure of a particle created less roughness than that of the original surface of the particle prior to the test.

6.0 PROCTOR TEST

When any kind of material is under an amount of stress that exceeds the strength of the material, the material will fail. Although a material fail when the applied stress is greater than the strength of material, the crushing behavior at the time of failure differs depending on the material considered. For example, when sand is under uniaxial compression stress, it will be more compact. And most other granular materials will also be compacted under this type of stress. In the case of sand, crushing behavior of each sand particle is less important than how all of the sand particles as a group behave. On the other hand, in the case of granular material, the crushing behavior of each particle is important as well as the behavior as a group. This is because when the mass of granular material such as gravel is under stress, the fragmentation of each particle is more visible and influences the changes in property than sand material. Using fractal analysis the change in the roughness of particles and the size distribution of the particles were determined. In this experiment, the equipment of a modified proctor test was used to apply stress to granular material.

6.1 EQUIPMENT

The weight of the hammer used in this experiment was 10.5 lb and the size of mold used was 10 cm in inner diameter and 11.5 cm in height. The granular material used in this experiment was the same type of sandstone as was used in the other tests. Sieves that were used in this test are listed in Table 6.1.

Table 6.1: Sieve opening size.

	Opening Size
Sieve	mm
Sieve#1	38.1
Sieve#2	16
Sieve#3	12.7
Sieve#4	9.5
Sieve#5	6.35
Sieve#6	4.76
Sieve#7	2.36

6.2 PROCEDURE

Proctor tests were performed using different numbers of blow counts. The number of blows applied in each test were 25, 50, and 100 blows per layer, respectively. Proctor tests with these three blow counts were performed on both the dry and wet samples. Wet samples had been immersed in water for 4 days. The granular material used was randomly picked. The grain size distributions of the samples were determined before and after the tests were performed to

determine the changes in fragmentation fractal dimension, D_F. Also the pictures were taken to determine the roughness fractal dimension, D_R.

6.3 GRAIN SIZE DISTRIBUTION PLOT

6.3.1 Dry Samples

First, dry samples were tested to see the difference in fragmentation behavior by performing tests with different numbers of blows applied. Figure 6.1, 6.2, and 6.3 show the grain size distributions of the dry samples before and after the tests for 25, 50, and 100 blows per layer respectively. Just from visual comparison of these three plots, differences in the change in grain size distribution before and after the test were noticeable.

The original grain size distribution of the samples tested with 25 blow counts per layer showed more weight passing 16.0 mm and 12.7 mm sieve opening size than the other samples tested with two other blow counts. Before any tests were performed the samples which were tested with 50 and 100 blows per layer had almost the same grain size distribution. The grain size distributions of the three samples after the test showed that the sample tested with 100 blows per layer had a much greater amount passing through the two large sieve openings mentioned before. But sample tested with 50 blows per layer still had fewer fines at these two sieve opening size than sample tested with 25 blows per layer. On the other hand, amount of particles passing sieve openings of 6.35 mm or smaller were almost the same for all three samples before the test. But change of amount of finer after the test was significantly different for all three samples.

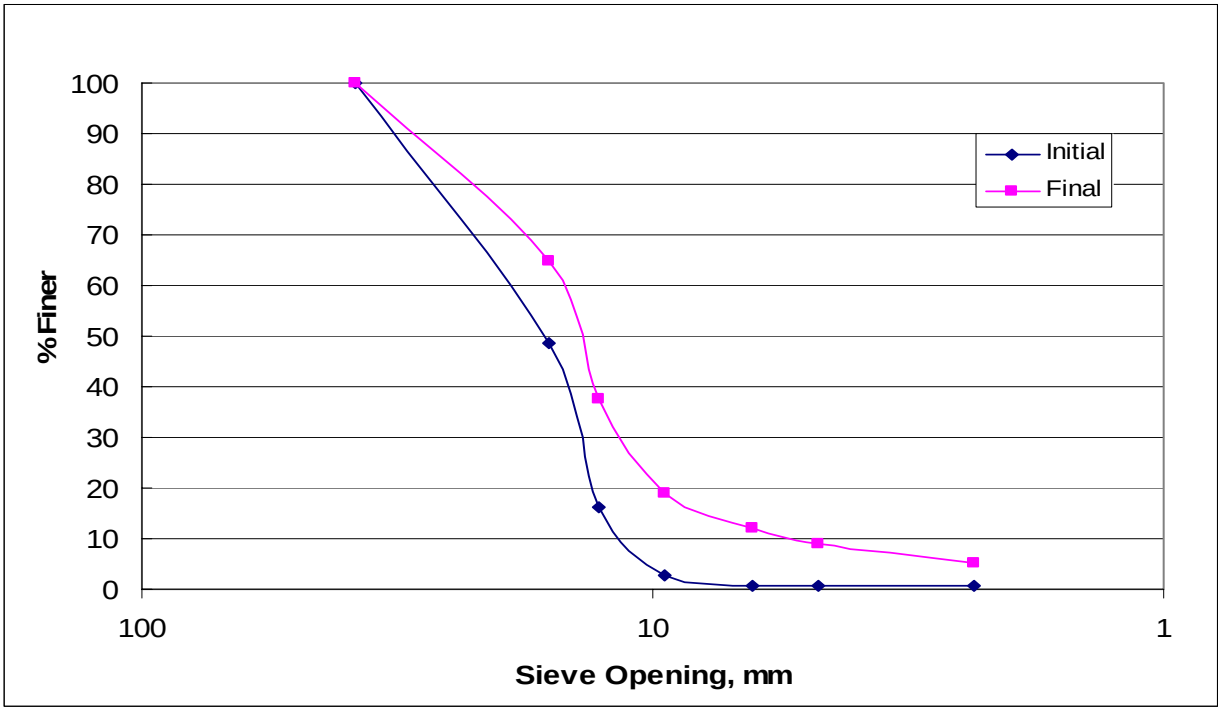

Figure 6.1: Grain size distribution of dry sample before and after the test with 25 blows/layer.

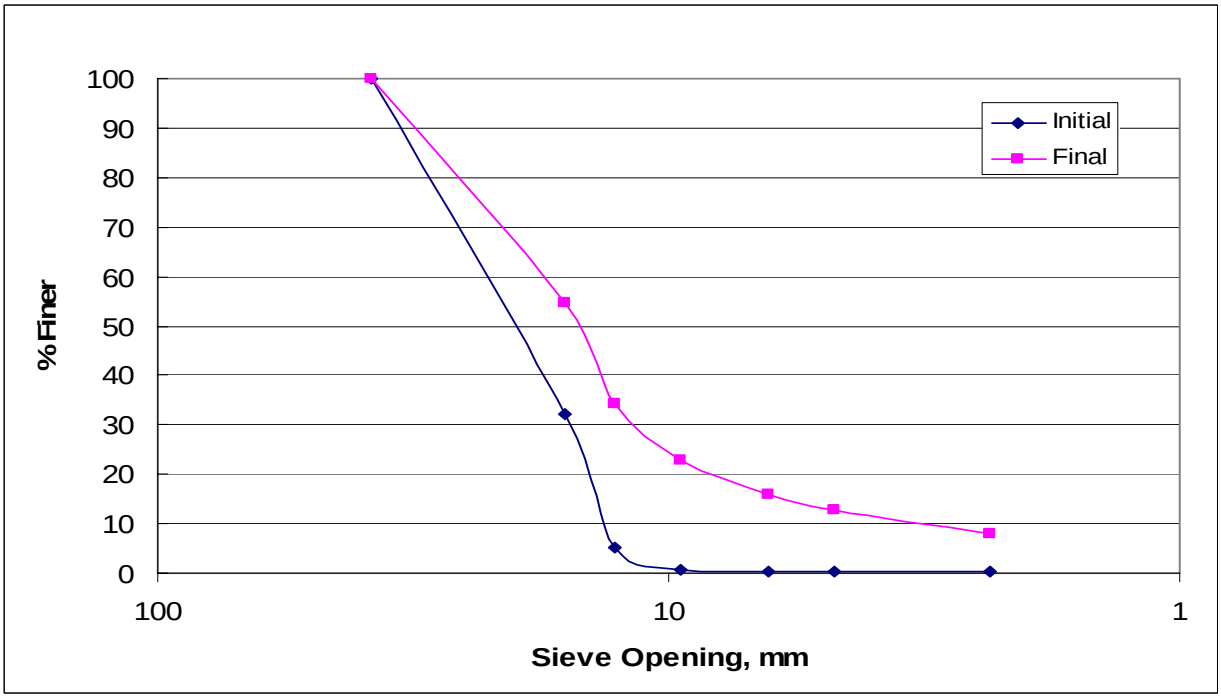

Figure 6.2: Grain size distribution of dry sample before and after the test with 50 blows/layer.

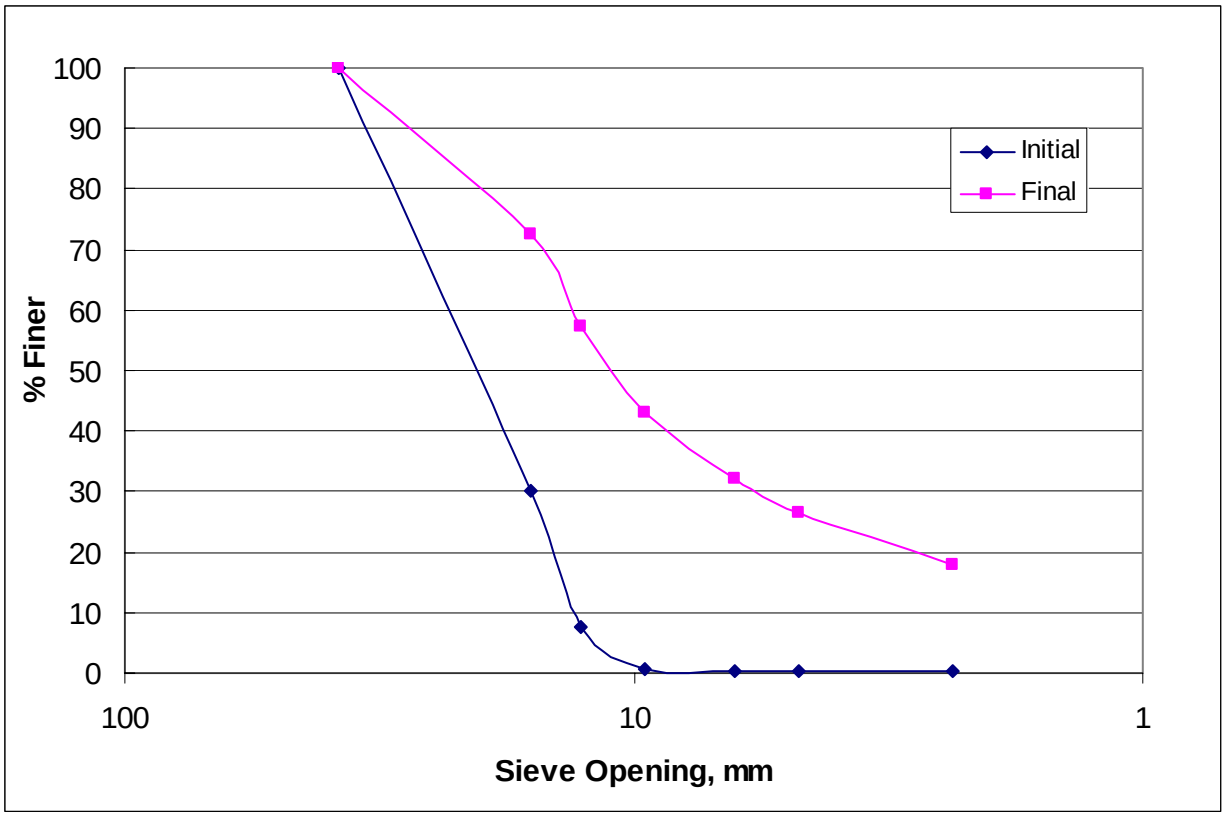

Figure 6.3: Grain size distribution of dry sample before and after the test with 100 blows/layer.

6.3.2 Wet Sample

The following three figures, Figure 6.4, 6.5, and 6.6, show the grain size distribution of wet samples with the same three number of blow counts as dry samples. These figures show that the basic characteristic of change in grain size distribution was similar to what it was for dry samples. As discussed in the previous chapter, the strength of granular material decreases when it is wet or saturated. For the sandstone used in this research, the average reduction was found to be about 14%. Thus, wet samples were expected to have greater amount of crushing. However, from a visual comparison of the grain size distribution, the crushing behavior appeared to be almost the same in the dry and wet samples. One major difference was observed between dry and

wet samples in the sample with 50 blow counts per layer. As observed in the dry sample with 50 blow count per layer, the amount of particles passing through the sieve opening of 6.35 mm or smaller sieve opening was almost the same as the amount found with the sample receiving 25 blow counts. However, in the wet sample, the amount of particles passing these two sieve opening sizes was much greater in the sample that received 50 blow counts. Even considering that the original grain size distribution was not exactly the same, the resulting grain size distributions of these two samples were very different. This result suggests that saturation had some minor influence in the process of crushing.

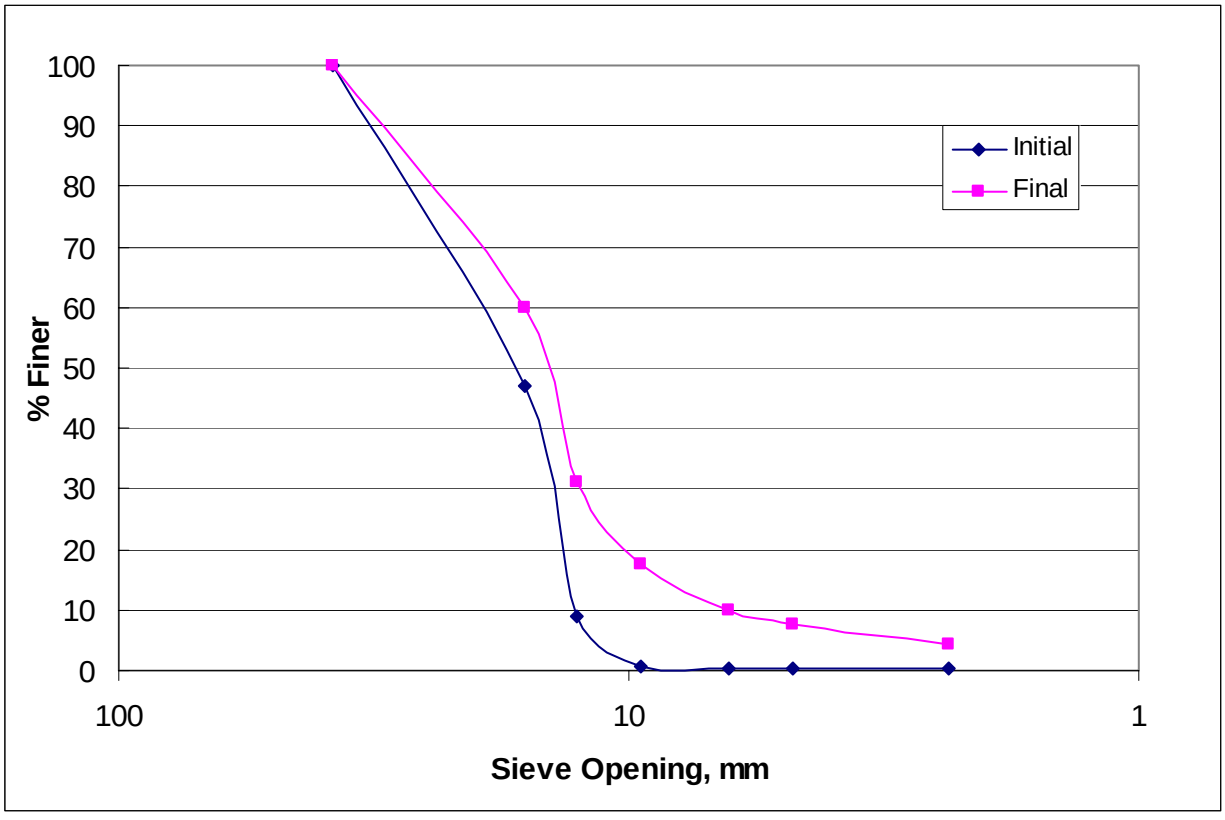

Figure 6.4: Grain size distribution of wet sample before and after the test with 25 blows/layer.

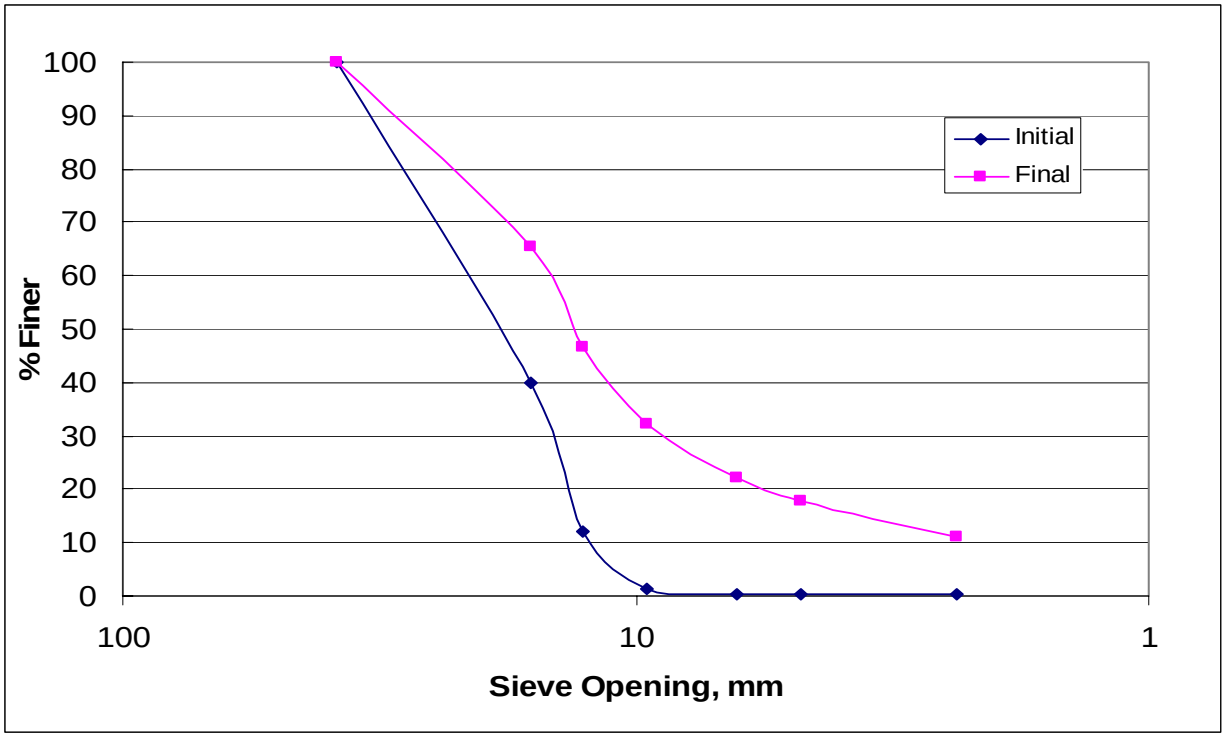

Figure 6.5: Grain size distribution of wet sample before and after the test with 50 blows/layer.

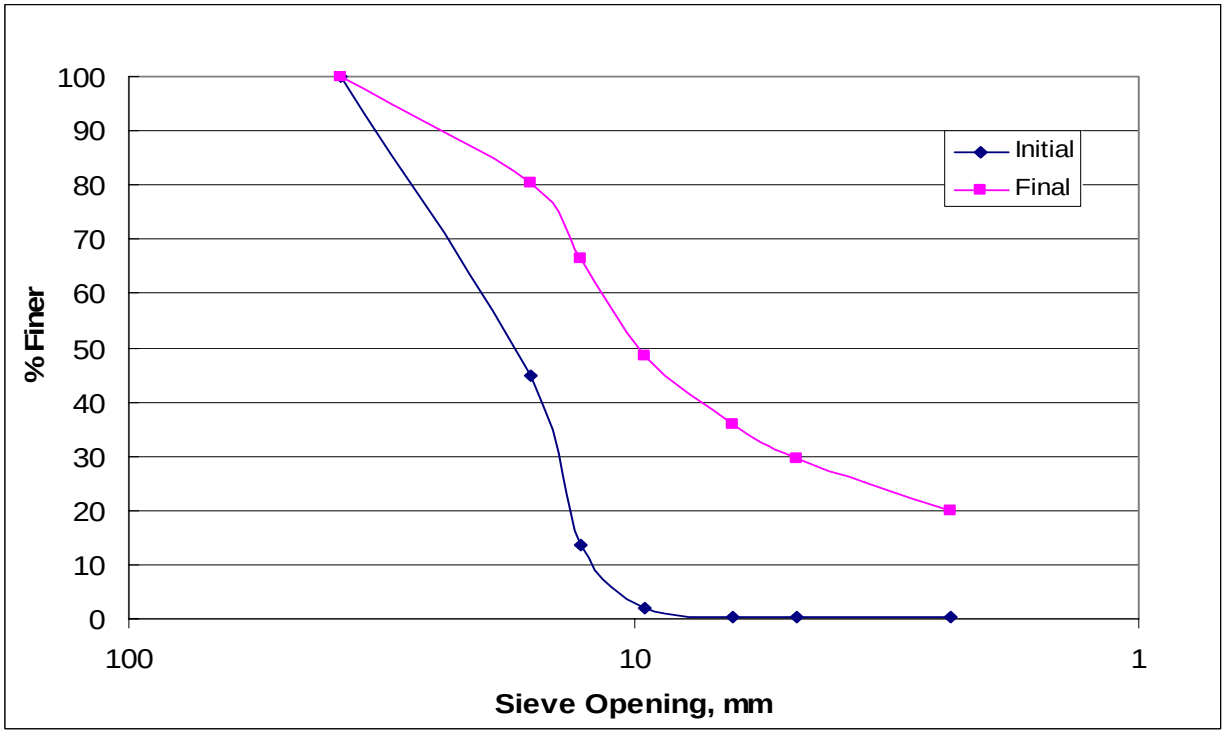

Figure 6.6: Grain size distribution of wet sample before and after the test with 100 blows/layer.

6.4 FRAGMENTATION FRACTAL DIMENSION, D_F

Fractal analysis was used for analysis of this test. First, the fragmentation fractal dimension, D_F, was determined to understand the particle size distribution of each sample. Since the influence of saturation could not be determined well from the plot of grain size distribution, D_F determined would make it possible to understand what had happened during the test. Table 6.2 summarizes the result of D_F determined before and after the test for each of the 6 samples tested.

Table 6.2: Summary of fragmentation fractal dimension, D_F, of 6 samples before and after the tests and the difference between two states.

	Before	After	Difference
25 BLOW/layer (Dry)	0.7172	1.8321	1.1149
50 BLOW/layer (Dry)	0.7172	2.0353	1.3181
100 BLOW/layer (Dry)	0.6407	2.3387	1.6980
25 BLOW/layer (Wet)	0.4703	1.7577	1.2874
50 BLOW/layer (Wet)	0.6099	2.1569	1.5470
100 BLOW/layer (Wet)	0.6165	2.3705	1.7540

Many characteristics can be seen from Table 6.2. First of all, the original values of D_F before the tests were performed should be analyzed to understand the basic difference before performing further analysis. As reflected in this table, the original values of D_F were found to be different for each sample. The highest value of D_F was 0.7172, and the lowest value was 0.4703. This was quite a difference and the resulting D_F could have been affected by this difference in original

value. The original values of D_F for the dry samples subjected to 25 and 50 blows per layer were the same, but this was a coincidence, and no attempt was made to have these two values be the same.

Second, the values of D_F after the test should be analyzed. The values of after the test show similar trends for both dry and wet materials. The table shows that D_F increases as the number of blow counts applied to each sample increases. This result indicates that as more blows were applied to the samples, samples tended to become more fractal, as was expected. For example, the original value of D_F for the dry sample with 100 blows applied to each layer was 0.6407 and the original value of D_F for the dry sample with 25 blows applied to each layer was 0.7172. However, after the test, the sample with 100 blows applied to each layer had a much greater value of D_F than the sample with 25 blows applied.

In further analysis, the change of D_F before and after the test should be discussed. In the right hand column of Table 6.2, the difference of D_F before and after is summarized for all the samples. First, it can be seen that for both dry and wet samples, the difference of the D_F increases as the number of blow counts increases. Analysis of the "Difference" column of Table 6.2 revealed a phenomenon similar to one earlier found in the analysis of the "After" column in Table 6.2 In the previous analysis, it was determined that D_F increases as the applied number of blows increases; however, in this analysis, it can be determined that the change of D_F also increases as the number of blow counts increases. The result of this analysis would reinforce the result from previous analysis that the original D_F had less influence on the change in the size distribution of samples to the final D_F than the number of blows applied.

This difference in the rate of change in D_F can be used to determine the influence of saturating the samples before the test. Another key characteristic was the difference in the rate

of change in dry and wet samples. For all three different numbers of blow counts applied to samples, it was determined that the difference of D_F for saturated samples was greater than for dry samples. This result suggested that wet samples had undergone more abrasion or fragmentation and created a greater amount of small particles. This was what was suggested by the results of the point load test even though it was not so clear from the grain size distribution curve.

In conclusion, by analyzing the value of $D_{F,}$ many information of size distribution change can be seen in quantified value, which grain size distribution plot cannot provide. This information includes such items as an analysis of D_F that determines the influence of saturation on the evolution of granular material. But at the same time, it should be noted that a simple visual comparison of the grain size distribution plot allows many of the same characteristics to be identified.

6.5 ROUGHNESS FRACTAL DIMENSION, D_R

The roughness of samples was measured using fractal analysis. From each of the samples, 20 particles were picked and their area and perimeter were measured. However, unlike $D_{F,}$ the original values of D_R for each of the samples that were tested were not determined before the test. Thus, using 50 different particles of the same material, which were in their original state, one value of D_R was determined. This determined value was used as the original D_R for all six samples. By using 50 particles of the material instead of 20 particles, the original D_R for all 6 samples should be sufficiently represented.

Table 6.3 summarizes the result of D_R after the tests. From this table it can be seen that for dry samples, the D_R increased as the number of blows applied to the sample increased. But by assuming all the samples had original D_R of 1.0240, a different process of fragmentation can be found. For the sample with 25 blows applied to each layer, it was found that the D_R decreased from its original value. The main reason why the D_R decreased would be because of the total failure of particles. From the roughness fractal analysis of particles done in the point load test, it was determined that the total failure caused the D_R to decrease. This could also be caused by the failure of asperities of the particles. Thus, the relatively large edges on the particle surface were fragmented from the surface of particles and created a smoother surface at the area of the surface where asperities were removed. Compared to this value of $D_{R,}$ the D_R of the sample subjected to 50 blows on each layer increased. This could be because the sample was subjected to a greater amount of abrasion and fragmentation. Since many of the contacts that particles originally had could be at asperities, once these asperities were removed, the main body of the particles were subjected to more abrasion and fragmentation making the surface of particles rougher again. This abrasion could also have happened on the surface created by the total failure of the particle. And when 100 blows were applied to each layer, particles became even rougher than when 50 blows were applied to each layer. The reason why the D_R increased might be because the particles were subjected to even greater amount of abrasion and fragmentation, thereby, making the surface of the particles even rougher.

On the other hand, in the saturated sample more reduction in D_R was observed for all numbers of blow counts. This was completely the opposite of the change in D_R for dry samples in which the D_R didn't decrease. As determined by the point load test, the strength of granular material decreases when it is saturated. And as determined from the analysis of D_F in the

previous section, a greater amount of smaller particles were created in saturated samples than in dry samples, so there was more total failure or splitting of particles and a smoother surface was created. Another explanation for this reduction of D_R would be that the granular material became more plastic when it was saturated and any type of failure that occurred on saturated granular material created a smoother surface. This phenomenon can be observed with the crushing of glass beads. Glass beads are plastic and brittle, and when they are crushed, the failure surface produced is very smooth.

Table 6.3: Summarized table of roughness fractal dimension, $D_{R,}$ after the test.

	D_R
Original	1.0240
25 blow/layer (Dry)	0.9966
50 blow/layer (Dry)	1.0135
100 blow/layer (Dry)	1.0489
25 blow/layer (Wet)	1.0029
50 blow/layer (Wet)	0.9712
100 blow/layer (Wet)	0.9638

6.6 SUMMARY

In conclusion, as expected, it was determined that for both dry and wet samples the change in the grain size distribution increased as the applied number of blows increased. The grain size distribution plot and the result of analysis of fragmentation fractal dimension, D_F, offer evidence of this phenomenon. The influence of saturation on granular material was not clearly evident

from the grain size distribution plot, but it was very clear from analysis of D_F. The roughness fractal dimension, D_R, which was calculated after the test indicated that saturation influenced the change in roughness during crushing. The roughness first decreased then increased again for the dry sample. On the other hand, when the granular material was saturated, the roughness decreased as the number of applied blow counts increased.

7.0 BY LAYER EXPERIMENT

The purpose of this experiment was to examine the crushing behavior of granular materials in different layers such as top, middle and bottom layer under different loadings. The result obtained from a previous proctor test considered the whole sample as just one sample, but in this section, each sample was separated into three different layers, each of which was considered separately. Also, in this experiment, samples with different particle sizes were tested to study the influence of the original particle size on evolution of the granular materials.

7.1 PROCEDURE

First, the granular samples were placed in the mold to the height of approximately 10.5 cm and then samples were removed from the mold. In the process of removing them, the sample was separated into top, middle, and bottom layers of approximately 3.5 cm each. Then each sample layer was separately processed through sieve analysis to obtain the grain size distribution. From the weight distribution, the fragmentation fractal dimension, D_F, was determined. Also 30 particles were taken out from each layer and pictures were taken. From this picture, the area and the perimeter of selected particles were obtained. After these necessary data were obtained, the samples were put back into the mold, and 100 blows were applied. After the blows were applied,

the total height of the 3 layers was reduced to about 7.5 cm. Thus, the new height for each layer was determined to be 2.5 cm. Then the sample was taken out of the mold in layers and the grain size distribution, fragmentation fractal dimension, and roughness fractal dimension for each layer was determined. This experiment was performed in samples with different particle sizes. The first sample consisted of the particles that were randomly picked. The second and third samples consisted of a specific size particles. Table 7.1 summarizes the original particle size.

Table 7.1: Table of initial particle size of each test.

Test #	Sample #	Original Particle Size
1	1	Random
2	2	16.0mm~38.1mm
3	3	12.7mm~16.0mm

7.2 VISUAL ANALYSIS OF THE TEST RESULT

7.2.1 Visual analysis of sample 1

The following three figures, Figure 7.1, 7.2, and 7.3**,** show the pictures of sample 1 that were removed from the mold after the test. The figures are the pictures of granular samples from the top, middle and bottom layers, respectively. By visually comparing these three pictures, different characteristics of crushing behavior can be noted even before any further analysis is performed. It must be noted that the large amount of fine particles in Figure7.3 was due to the difficulty of collecting these particles from top and middle layers in the process of removing the sample from the mold. Also, some of the fine particles might have migrated from the top and middle layers

and their original location couldn't be known. This same problem occurred with the other samples too.

First, the different number of remaining large particles is apparent from observation. By observing Figure 7.1, the picture of the top layer of sample1, it can be seen that the number of large particles was much less than that of, Figure 7.2 and 7.3. And Figure 7.2, the picture of the middle layer of sample 1, had the largest number of large particles. It can also be seen that the top layer had the greatest amount of particles having a diameter of approximately 10 mm. Many of these particles could be the fragments of larger particles. Although it is hard to see from these figures, particles of this diameter on the top layer had fewer large angular edges. In other words, they were more spherical than the same sized particles from the other two layers. In the other two layers, particles of this diameter were flatter and had sharper edges. The spherical particles could have originated from the split of a body from larger particles that had been caused by a total failure. Once these particles were created, they either went through more process of abrasion and failure of asperity or another total failure. On the other hand, in the middle and bottom layers, there were fewer particles of the same size, and they were more angular. Also they were more flat than spherical. It could be assumed that these two lower layers were subjected to less crushing than the top layer. Hence, the total failure of particles happened less frequently and, consequently, fewer spherical particles of approximately 10 mm in diameter were created. The force required to create flat shaped fragments are much less than that required to cause a total failure because the failure planes that caused the flat shaped fragments were much smaller than the failure plane that caused total failure, so the force required is much less. For the same reason, the abrasion and failures of asperities were less. This result from a visual comparison of Figure 7.1, 7.2, and 7.3 indicates that the particles in the top layer experienced the most crushing, and

particles in the middle layer experienced the least crushing. The flat particles having a diameter of approximately 10 mm were observed only in the middle and bottom layers because the probability of particles with this shape and size surviving in the top layer is very low. In this chapter, large particles are defined as those having a diameter greater than 20 mm.

Figure 7.1: Material from top layer of sample 1 after the test.

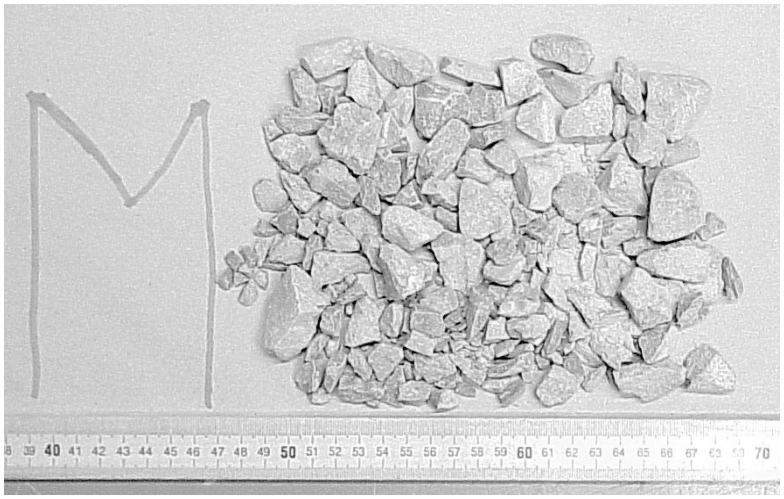

Figure 7.2: Material from middle layer of sample 1 after the test.

Figure 7.3: Material from middle layer of sample 1 after the test.

7.2.2 Visual analysis of sample 2

The following three figures, Figure7.4, 7.5, and 7.6, contain pictures of the top, middle, and bottom layers of sample 2 after the test, respectively. Sample 2 originally consisted of only particle sized between 16.0 mm and 38.1 mm. Although, the original sample sizes of the three layers were very similar, as can be seen in the pictures, the final composition of each layer was very different. As with sample 1, in Figure 7.4, it can be seen that there were many particles having a diameter of about 10 mm in the top layer. And there were many fewer similar sized particles in the other two layers. From Figure 7.5, it can be seen that the middle layer of this sample went through almost very little crushing of any type. There were relatively many fines in this layer, but it could be assumed that some of these fines fell down from the top layer.

Figure 7.4: Picture of top layer of sample 2 after the test.

Figure 7.5: Picture of middle layer of sample 2 after the test.

Figure 7.6: Picture of bottom layer of sample 2 after the test.

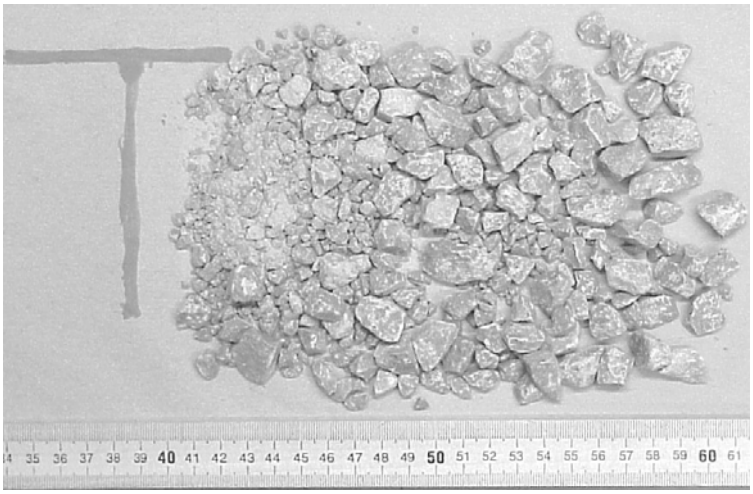

Figure 7.7: Picture of top layer of sample 3 after the test.

Figure 7.8: Picture of middle layer of sample 3 after the test.

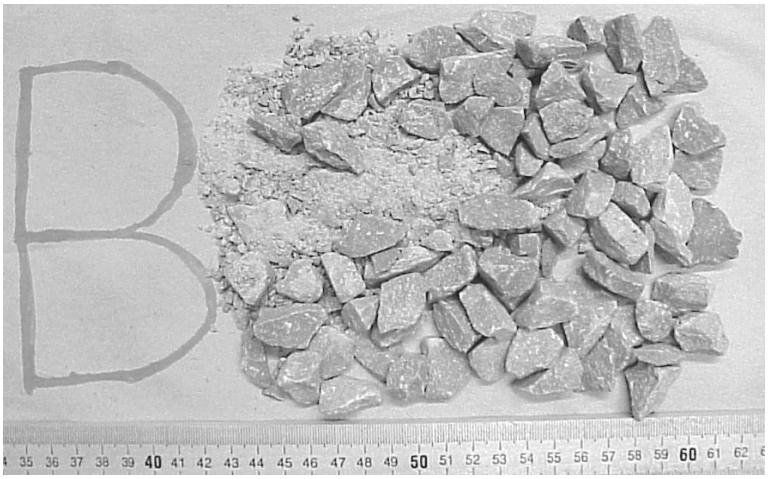

Figure 7.9: Picture of bottom layer of sample 3 after the test.

7.2.3 Visual analysis of sample 3

Figure 7.7, 7.8, and 7.9 are pictures of the top, middle and bottom layers of sample 3 after the test, respectively. From these three pictures, the great amount of fines created in this sample during the test can be noticed. Since the particles comprising this sample were the particles that passed through the 16.0 mm sieve opening but were retained in the 12.7 mm sieve opening, the total number of contact established between the particles was much greater than sample 2, increasing the chance of abrasion and resulting in a great amount of fines. A characteristic noted with the visual inspection of the previous 2 samples can again be noticed in this sample: the top layer suffered the most crushing and the middle layer suffered the least.

7.3 GRAIN SIZE DISTRIBUTION PLOT

7.3.1 Grain size distribution plot for sample 1

The first test was performed on sample 1, which was the sample with randomly picked particles. Since sample was randomly picked, the grain size distribution of this sample was determined before the test was performed. Figure 7.10 shows the grain size distribution of sample 1 before the test and Figure 7.11 shows the grain size distribution of sample 1 after the test. From Figure 7.10 it can be seen that the grain size distributions were almost the same for all three layers before the test.

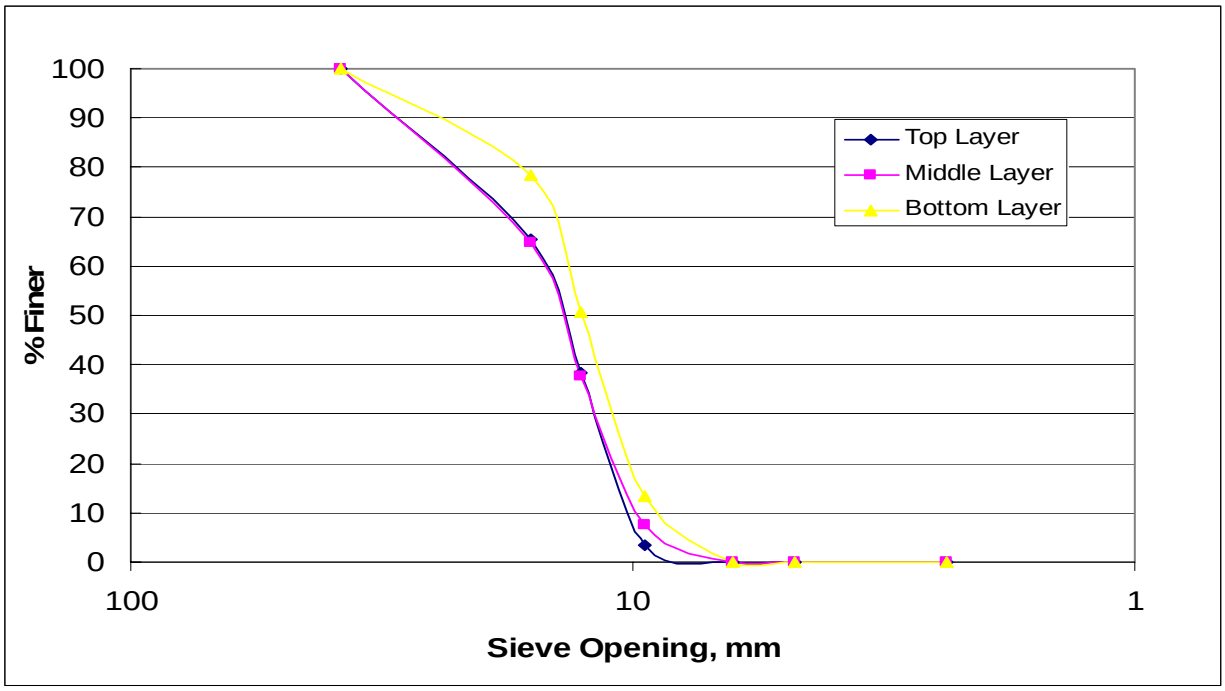

Figure 7.10: Initial grain size distribution of sample 1.

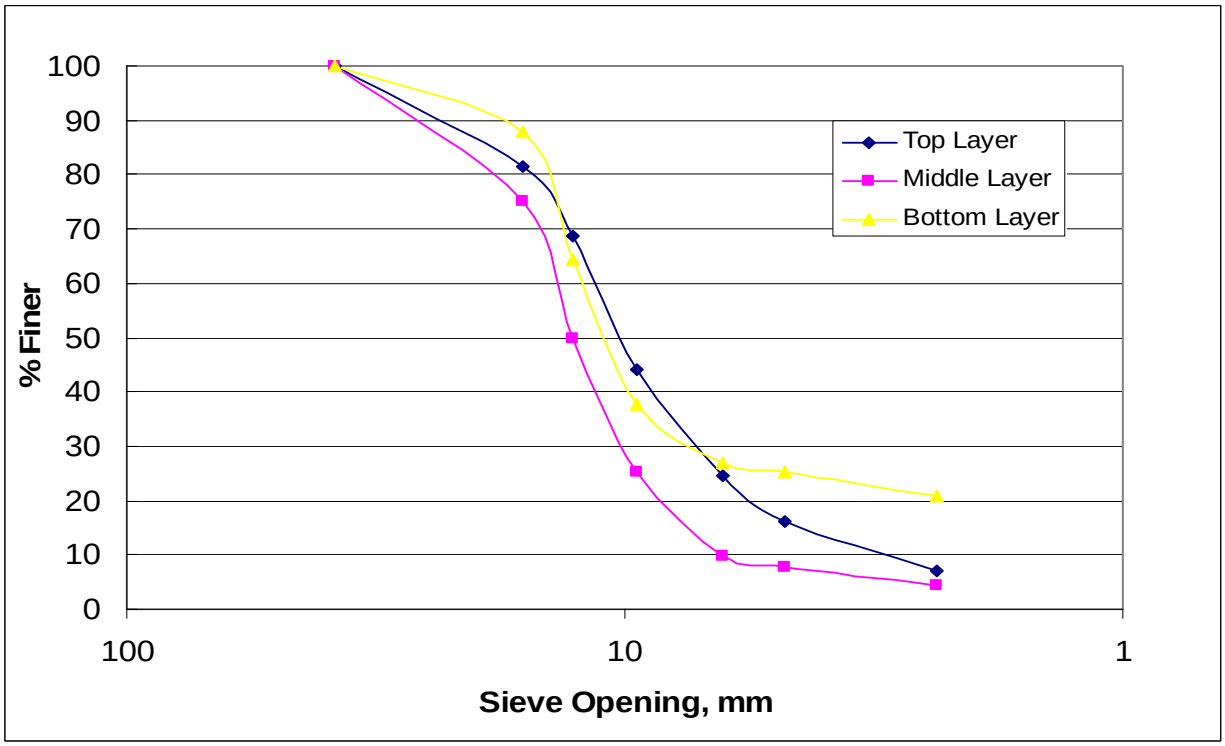

Figure 7.11: Final grain size distribution of the sample 1.

Figure 7.11 shows the grain size distribution of sample 1 after the test. By looking at this figure, it can be seen that the grain size distribution had became distinct for each layer. From Figure 7.10, it was determined that before the test, each layer had a similar grain size distribution, but after the test, the grain size distribution for each layer became very different. The middle layer seems to have had the least amount of crushing, and the top and bottom layers had a somewhat similar amount of crushing. This result is the same as the result obtained from a visual comparison of the pictures.

As mentioned earlier, many of the fines on the bottom layer could have originated in the top and middle layer and migrated to bottom layer during the test. Also as mentioned, the difficulty of recovering these fines might have contributed to this relatively large amount of fines in the bottom layer. Thus, the amount of fines that pass through the 2.36 mm sieve opening size doesn't accurately represent the actual value of fines produced in during the test.

As mentioned earlier, the layer that received the least crushing was the middle layer. The top and bottom layers received similar amounts of crushing. The following three figures, Figure 7.12, 7.13, and 7.14, show the initial and final grain size distribution of each layer. By looking at each of them, the difference in the degree of crushing each layer was subjected to can be seen.

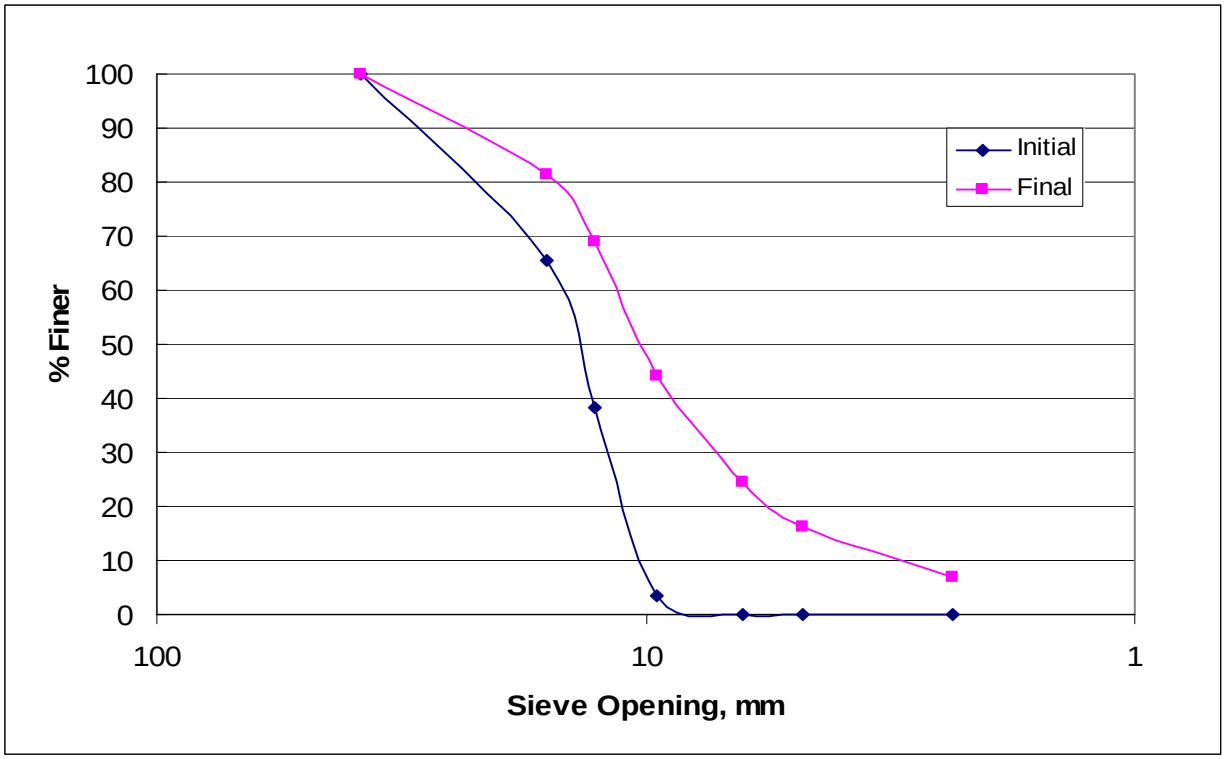

Figure 7.12: Initial and final grain size distribution of top layer of sample 1.

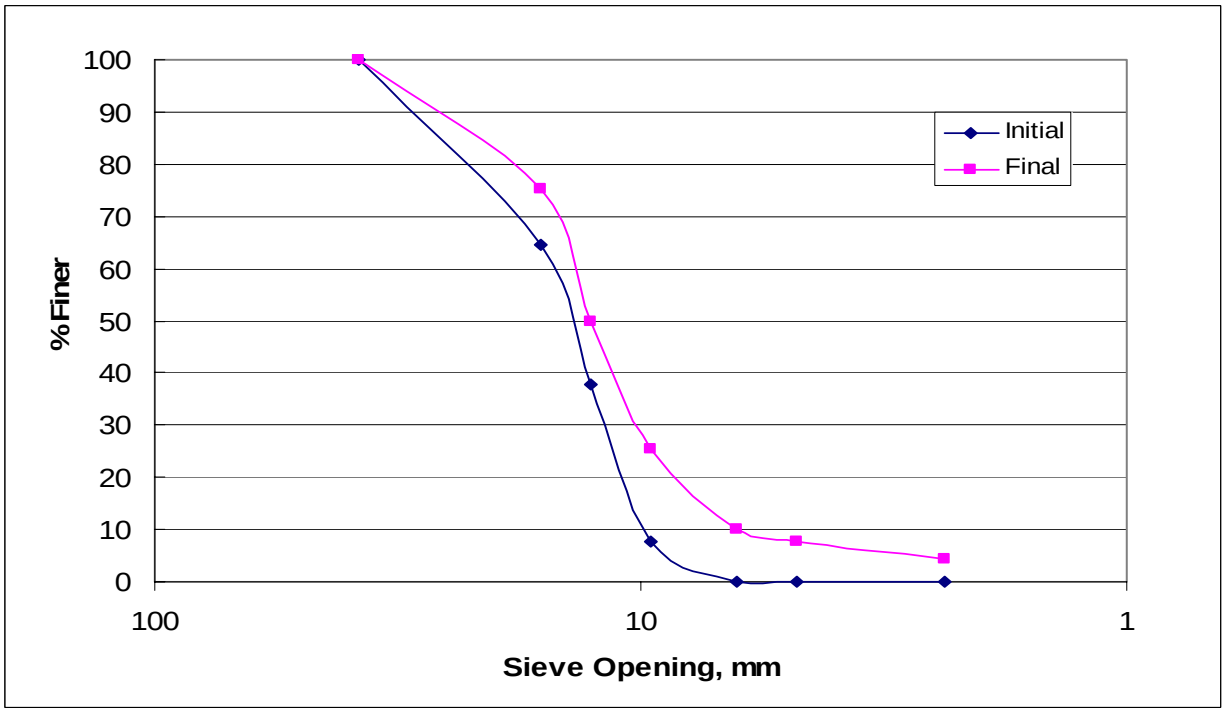

Figure 7.13: Initial and final grain size distribution of middle layer of sample 1.

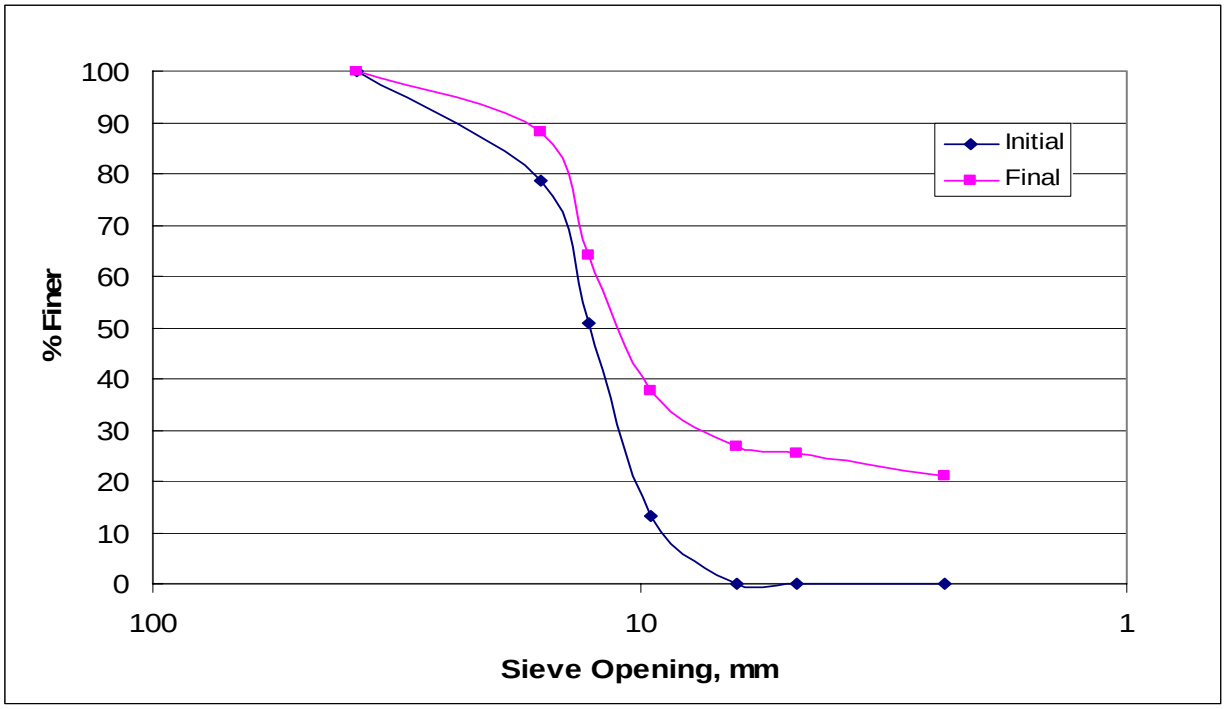

Figure 7.14: Initial and final grain size distribution of bottom layer of sample 1.

7.3.2 Grain size distribution of sample with specific original particle size

As previously stated , sample 2 and sample 3 were consisted of specific initial particle diameter, $d_{initial}$. Sample 2 was consisted of the particles that had $d_{initial}$ between 16.0 mm and 38.1 mm. And sample 3 was consisted of the particles that had $d_{initial}$ between 12.7 mm and 16.0 mm. The following two figures, Figure 7.15 and 7.16, show the plots of grain size distribution for sample 2 and sample 3, respectively. From these two plots, it is evident that the percent finer of sample 3 was greater than percent finer of other two samples for all sieve opening sizes that are comparative. This result was as predicted before the tests were performed. Since the original particle size of sample 3 was smaller than that of sample 2, sample 3 ended up with more fine particles.

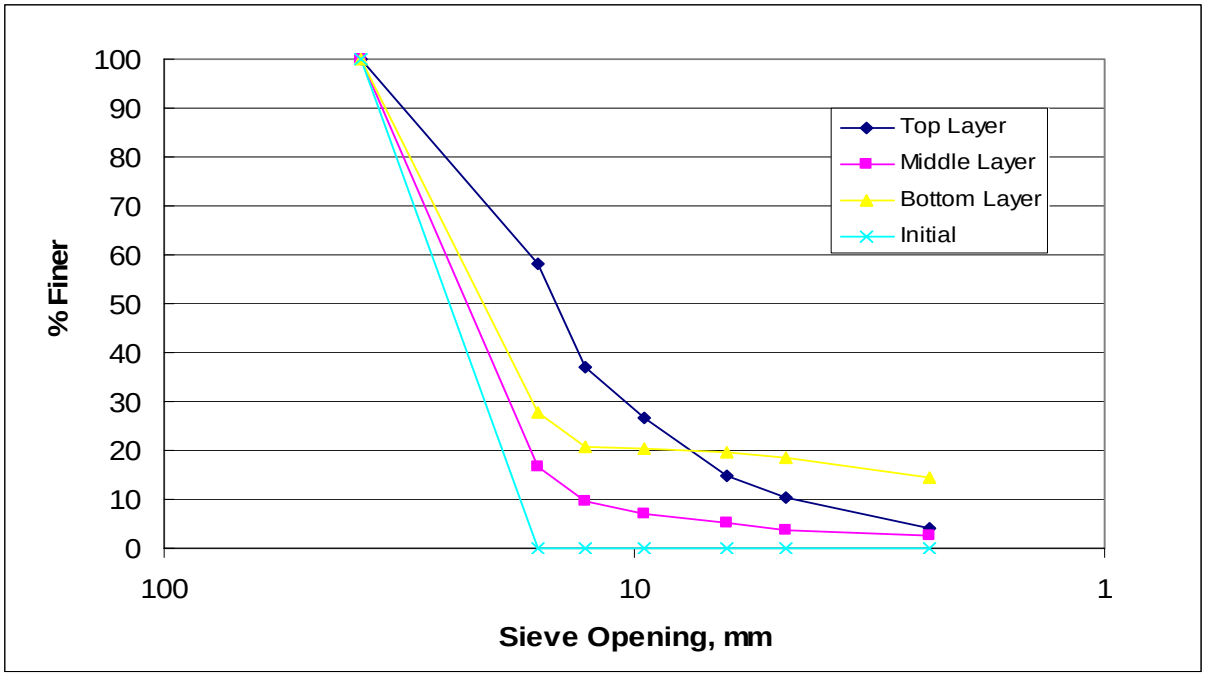

Figure 7.15: Initial and final grain size distribution of sample 2 with 16.0 mm< $d_{initial}$< 38.1 mm.

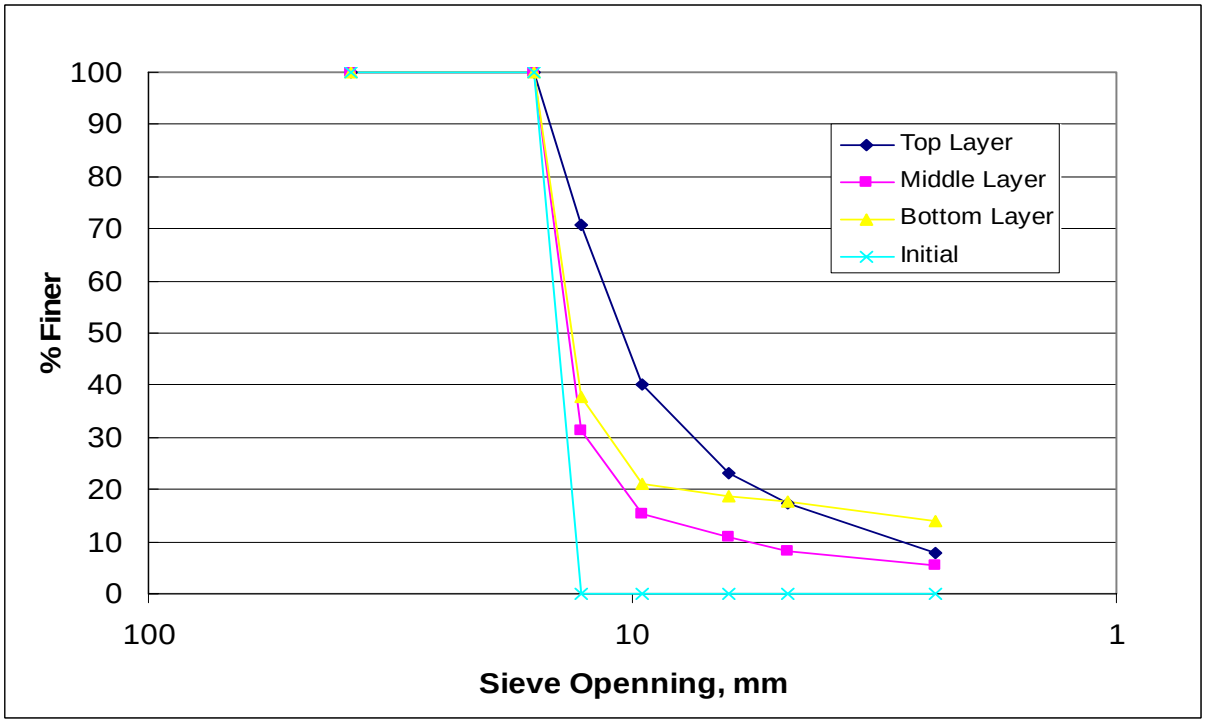

Figure 7.16: Initial and final grain size distribution of sample 3 with 12.7 mm< $d_{initial}$< 16.0 mm.

7.3.3 Comparison grain size distribution of sum of 3 layers

Table 7.2: Table of percent of particles passing through each sieve opening by weight after the tests.

Sieve	Opening Size, mm	Sample 1	Sample 2	Sample 3
Sieve#1	38.10	100.00	100.00	100.00
Sieve#2	16.00	81.17	34.20	100.00
Sieve#3	12.70	60.45	22.50	46.05
Sieve#4	9.50	35.29	18.12	25.14
Sieve#5	6.35	19.88	13.29	17.49
Sieve#6	4.76	15.87	10.82	14.42
Sieve#7	2.36	10.27	7.09	9.21
Pan	0.00	0.00	0.00	0.00

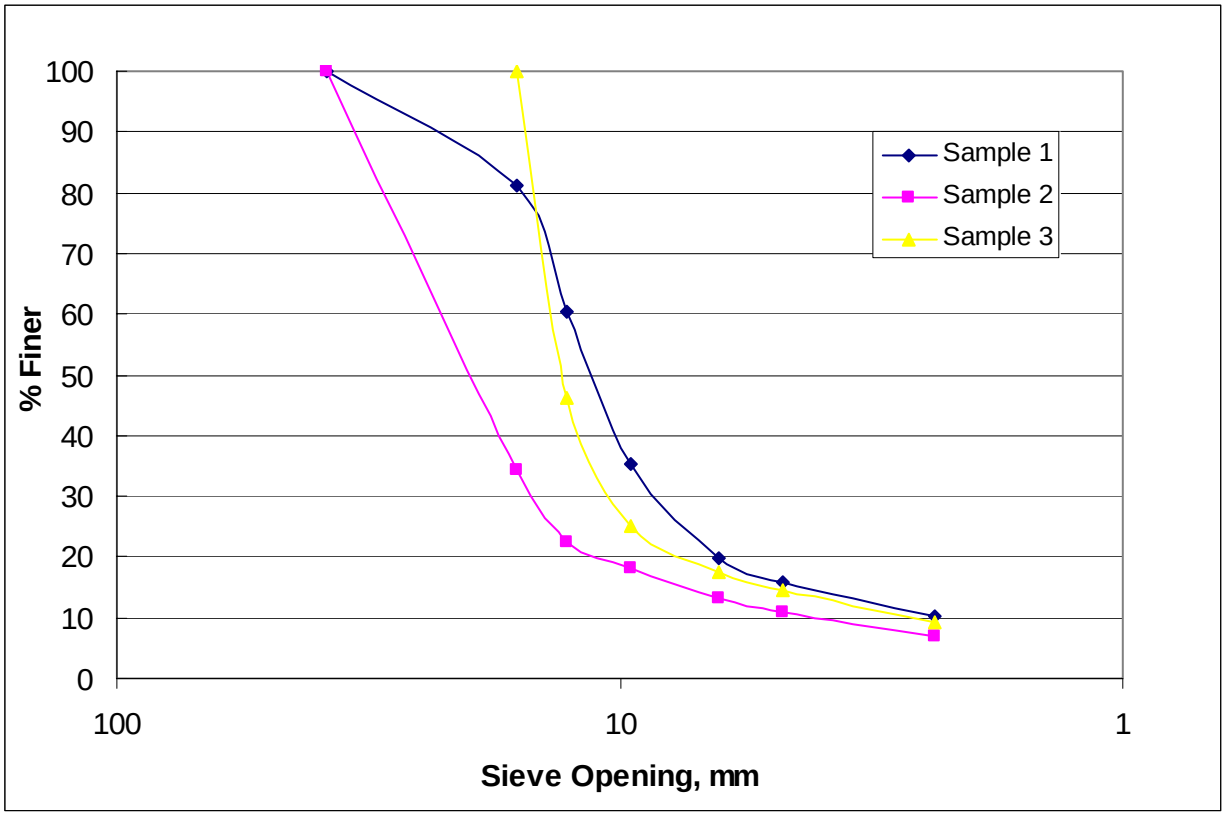

Figure 7.17: Grain size distribution plot of representing sum of all layers of 3 samples.

Table 7.2 summarizes the grain size distribution for 3 samples after the test, and Figure 7.17 shows the grain size distribution plot of the data from Table.3. This result shows that the percent finer for sample 2 after the test was always the lowest and the resulting percent finer for sample 1 was always the highest for all comparative sieve opening sizes. This was the expected result because sample 2 that had largest number of large particles. But this table shows another interesting characteristic that should not be ignored. The difference of weight of the particles passing through the same sieve opening size from the 3 samples decreased as the sieve opening size got smaller. For example, sample1 had 60.45% of its weight passing through sieve #3 (12.70 mm opening). And sample 2 and sample 3 from test 2 and test 3 had 22.50% and 46.05% of their weight passing through same sieve, respectively. At this sieve size, the percentage of weight of sample 1 that passed through was about 3 times the percentage of weight of sample 2 and 30% greater than sample 3. However, for sieve #7 (2.36 mm opening), the percentage of weight passing through for sample 1, sample 2, and sample 3 were 10.27%, 7.09%, and 9.21%, respectively. At this sieve opening size, the difference of percent finer was very little. The percent of sample1 passing this sieve opening size was 30% greater than that of sample 2 and only 10% greater than that of sample 3. The difference at sieve #7 was much less than the difference at sieve #3. For this experiment, the applied number of blows was constant for all three tests. Since number of blows was constant and the amount of small fines was similar regardless of the original particle size, the number of blows applied could have had a greater influence on abrasion. Thus, as more blows were applied, more collision occurs. This smaller difference of percent finer at the small sieve opening size suggests that the amount of fines produced was more influenced by the applied force, or in this case, the number of blows applied to the sample, and less influenced by the original particle size.

7.4 FRAGMENTATION FRACTAL DIMENSION, D_F

7.4.1 Sample 1 (Random sample)

Based on the grain size distribution of the sample obtained before and after the test, the fragmentation fractal dimension, D_F, was determined for each. Figure 7.18, 7.19 and 7.20 show the D_F of the top, middle, and bottom layers of the sample 1 before and after the test, respectively.

Figure 7.18 shows that the D_F of the top layer before the test was 1.0435 and after the test was 1.9667. Similarly, Figure 7.19 shows that the D_F before the test as 1.4360 and after the test as 1.6961 for the middle layer, and Figure.7.20 shows that the D_F before the test was 1.7957 and after the test as 2.3354 for the bottom layer. The values of D_F for the three layers before the test were not the same because the granular material in this sample was randomly chosen.

A characteristic noted in these D_F values is that D_F always increased after the test. The high value of D_F indicates that the sample is more fractal or has a greater amount of smaller particles. During the test, samples experienced a great deal of crushing and many smaller particles were produced. Thus, it was reasonable to have higher D_F values after the test. Another unique characteristic of this result was that the amount of change in the D_F was different for all three layers. The D_F for the top layer had almost doubled, while the D_F for the bottom layer had changed 0.5397 and the D_F for the middle layer had changed only 0.2601. The reason why this had occurred was because it was the top layer that experienced the most crushing. The bottom layer experienced less crushing than the top layer but more crushing than the middle layer.

The reason why the top layer experienced the most crushing and the middle layer experienced the least amount must be understood. The factor that caused this phenomenon was

the difference in the number of contact points or the coordination number of each particle. The particles in the top layer had direct contact with the dropped hammer; thus, all the stress was concentrated on one point on the particle. Consequently, this concentration of stress substantially lowered the probability of the particles surviving as compared to that of other two layers. For example, particles in the middle layer had a greater coordination number than the top layer. Thus, unlike the case of particles in the top layer, the stress applied to the particles in the middle layer was more distributed in nature than concentrated. The stress was transferred to the particles in the middle layer through multiple contacts. Thus, although the total stress applied to the particles in the middle layer might be as same as the stress applied to the particles in the top layer, the probability that the stress would exceeds the strength of the particles in the middle layer was less. Although the bottom layer had similar distributed stress applied to its particles, the bottom layer had greater amount of crushing than the middle layer. This is because the particles in the bottom layer had fewer contacts to transfer all the stress applied to the particle. It can be assumed that many of the particles in the bottom layer had only 1 contact with the bottom of the mold and this is the only support these particles had. Thus, even though the stress was applied to these particles in a distributed manner, the stress ended up being concentrated on one point. This situation was exactly the same in the case of particles in the top layer except that, in this case, the number of points where stress was applied and the number of support of particles had was switched.

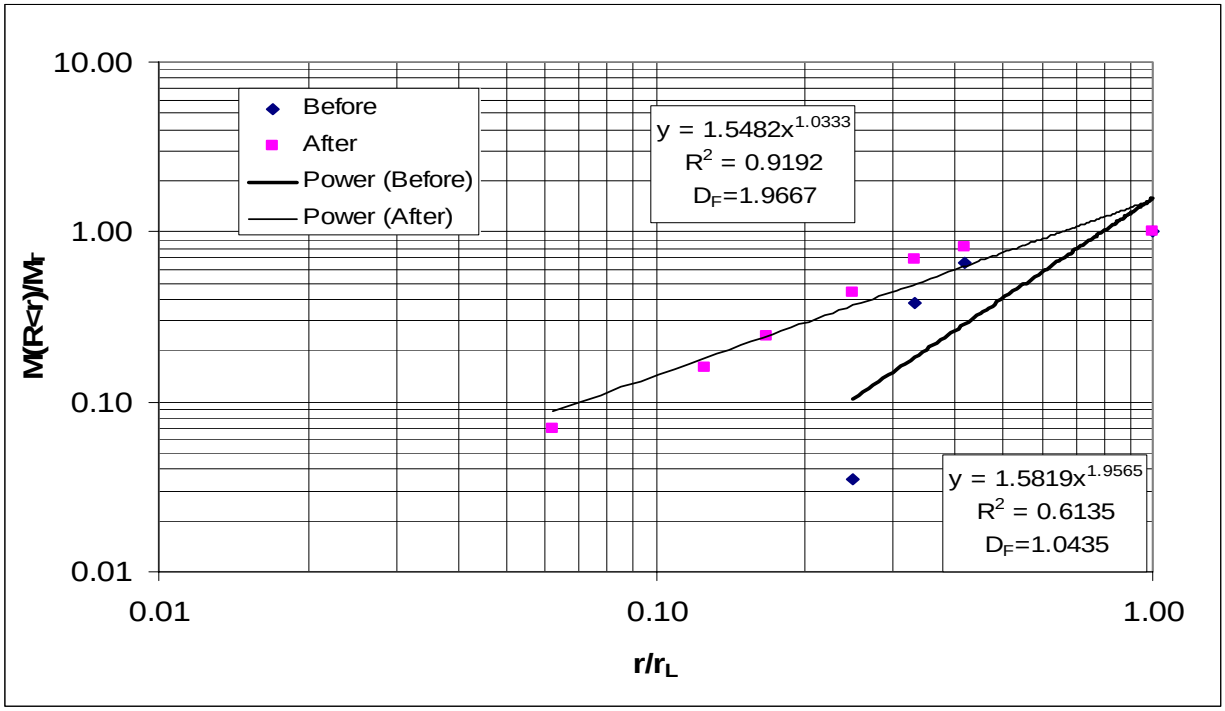

Figure 7.18: D_F of top layer of sample1 before and after the test.

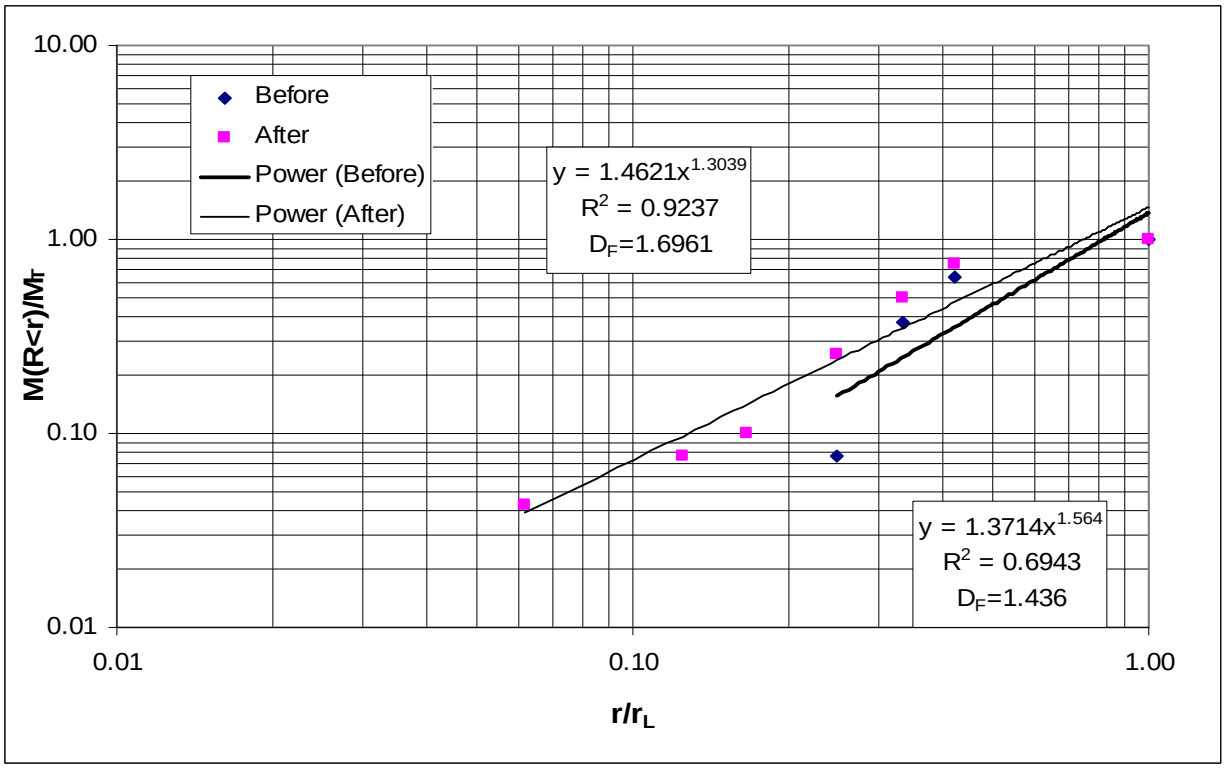

Figure 7.19: D_F of middle layer of sample 1 before and after the test.

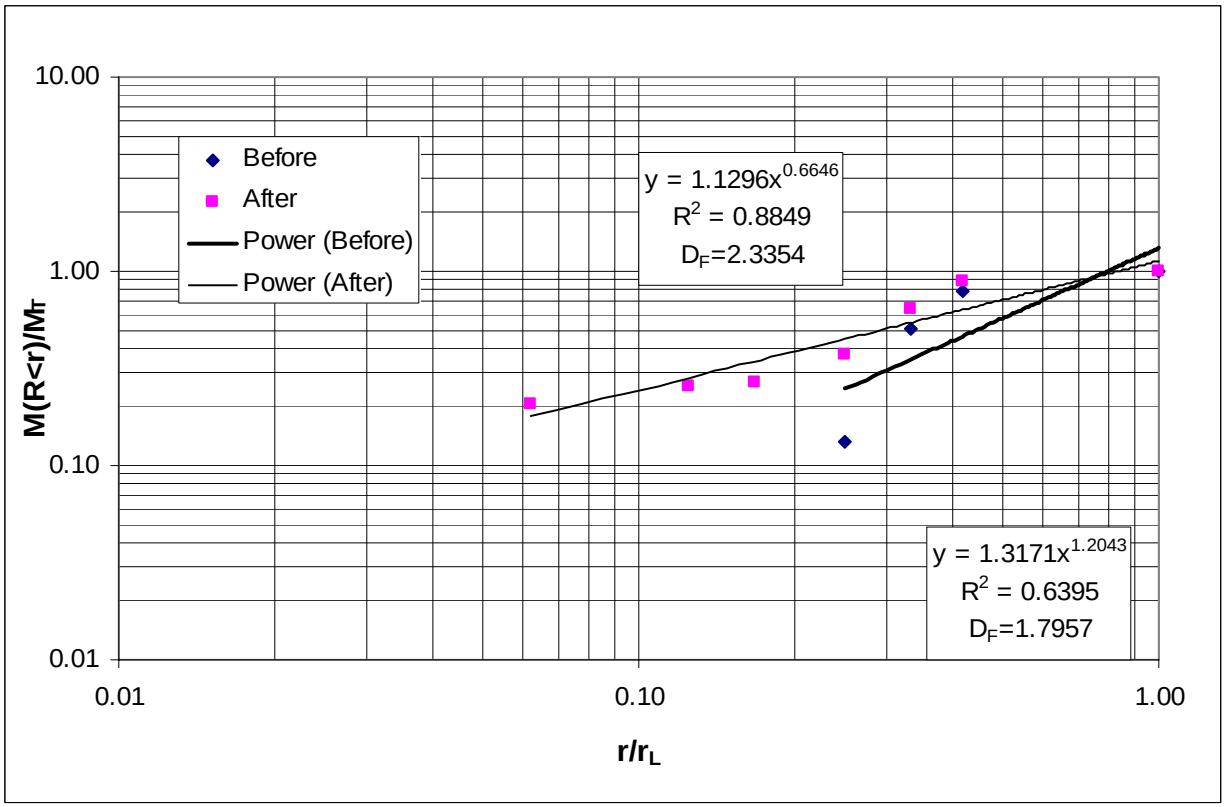

Figure 7.20: D_F of bottom layer of sample 1before and after the test.

However, this theory alone cannot explain why the bottom layer had less crushing than the top layer. If the situations of particles from the top and bottom layer were only inversed, the amount of crushing would be the same. This can be explained by referring to Figure 7.21 [(15)], which shows the force chain formed in the particles under uniaxial compression. The compression in this figure was a static load; thus, it is not exactly the same situation as that of the dynamic load used in this research. However, it can help explain why the crushing was less in the bottom layer than the top layer. As shown in this figure, some of the force chain in the picture was going to the exterior border. An exterior border was the mold of the in this research. This means that part of the stress applied to the sample was transferred to the mold and didn't reach the bottom of the

sample. Thus, this reduction of stress allowed more particles to survive in the bottom layer than the top layer.

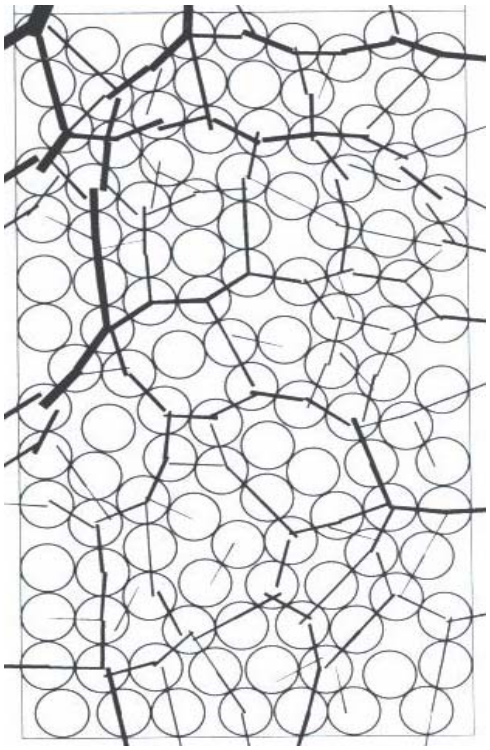

Figure 7.21: Picture of force chain under uniaxial compression obtained from DEM. (adapted from Lobo-Guerrero [14])

7.4.2 Sample 2

As shown in Table 7.1, the original diameter of the particles in sample 2 ranged between 16.0 and 38.1 mm. Figure 7.22, 7.23, and 7.24 show the D_F of the top, middle and bottom layers of this sample, respectively. The D_F of the sample before the test was performed is not shown here because the diameters of all of the original particle of sample 2 were in the range between two sieve size openings, and D_F could not be determined.

The D_F of the top, middle, and bottom layers of sample 2 were 1.8001, 1.7036, and 2.3814, respectively. Since the original size distribution of the samples were all the same, the D_F of this test result could not be analyzed in the same manner as the result from test 1, in which the analysis was focused on the change in D_F between before and after the test. On the other hand, since the original size distribution of this sample was the same for all layers, the comparison of D_F from after the test would be as meaningful as analyzing the change of D_F to determine the crushing behavior of the sample.

First, the D_F of the top layer of sample 2 was very close to that of the middle layer of the sample. In the analysis of D_F of test 1, it was determined that the top layer underwent the most crushing and the middle layer experienced the least crushing. But the determined D_F for sample 2 after the test indicated that the D_F of the top layer was only 0.1 higher than that of the middle layer. This might be because the migration of small fragment particles to the lower layer was increased in this test. This phenomenon may also have occurred on sample 1, but it was more apparent in test 2 because sample 1 was consisted of particles with different original diameters; thus, there were particles with diameters less than 16.0 mm, which could have filled up some of the void between particles larger than this. By contrast since sample 2 originally consisted of similar sized particles, there were no smaller sized particles to fill up the void space between larger particles. Thus, there was probably more migration of fines. This reason and also the imperfection of the recovering method of fines from each layer may explain why the D_F of the bottom layer of sample 2 was much higher than that of the other two layers. In sum, this is probably because many of the fine particles created during the test moved down to the bottom layer.

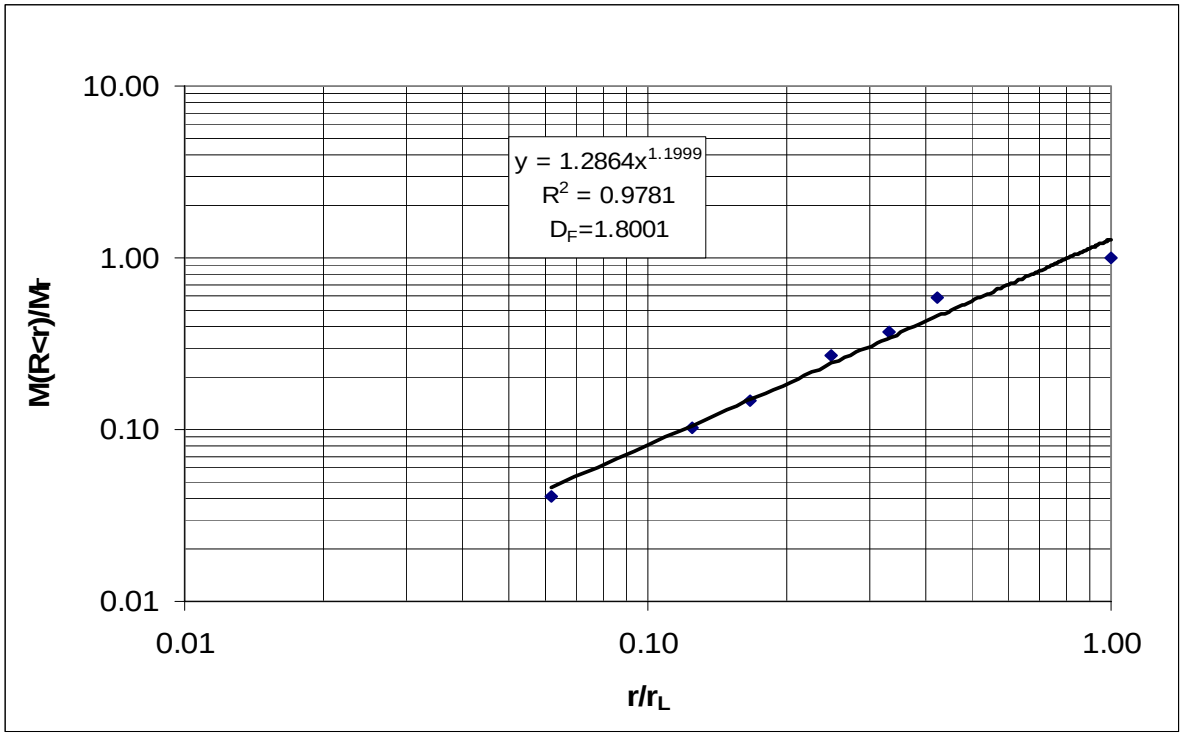

Figure 7.22: D_F of top layer of sample 2 after the test.

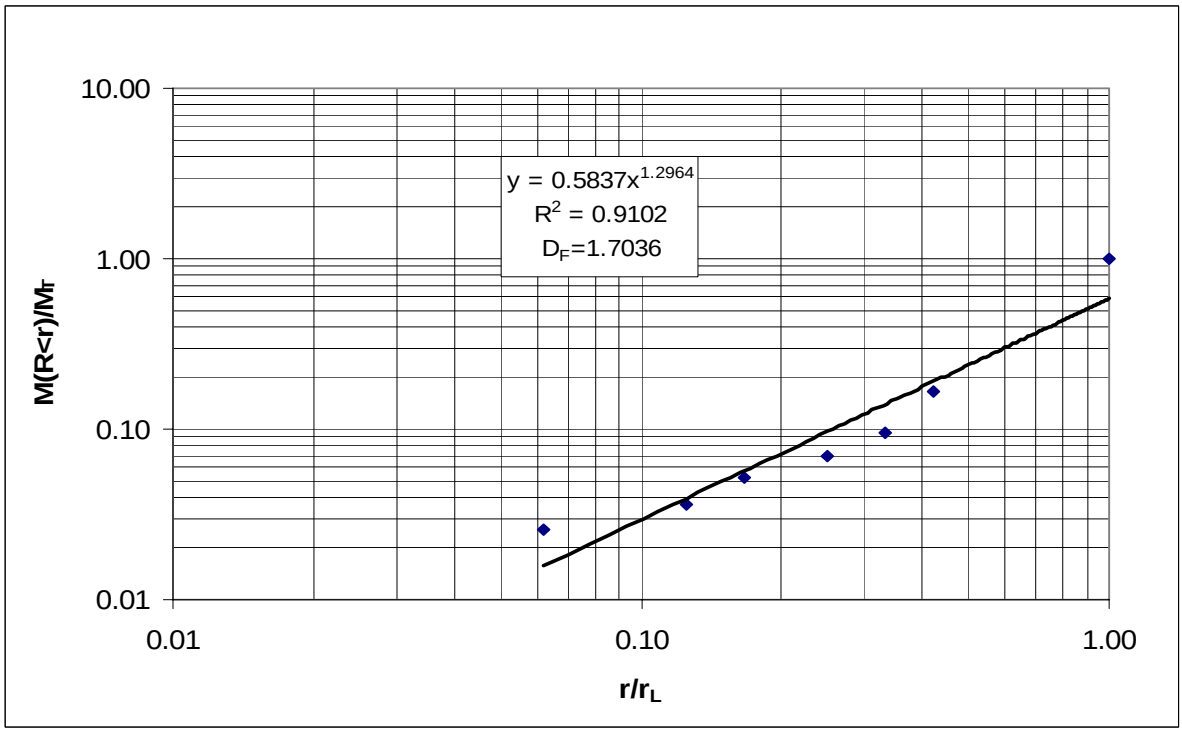

Figure 7.23: D_F of middle layer of sample 2 after the test.

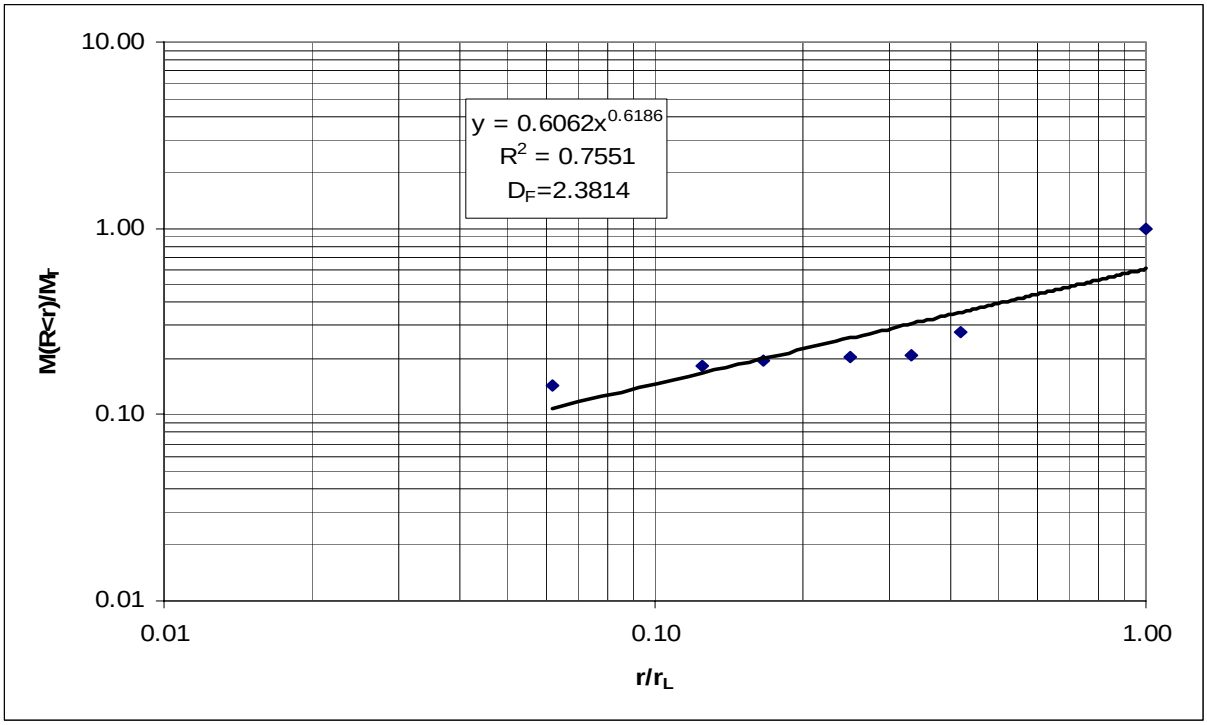

Figure 7.24: D_F of bottom layer of sample 2 after the test.

7.4.3 Sample 3

Test 3 was conducted with sample 3, which had original particle diameters between 12.7 mm and 16.0 mm. Before discussing the result of $D_{F,}$ it must be noted that in Figure 7.25, 7.26, and 7.27, r_L of 38.1 mm was used instead of 16.0 mm. According to Hyslip and Vallejo [5], r_L is the largest sieve opening size through which an entire particle can pass; thus, for this specific sample, the r_L must be 16.0 mm. However, in order to have the comparative result with sample 1 and sample 2, 38.1 mm opening was used as the largest sieve opening size.

The trend of D_F of sample 3 was different from that of sample2. In sample 3, the original particle size was much smaller than that of sample 2; thus, the total number of contacts in this sample must have been greater than in sample 2. This higher number of contacts consequently caused more abrasion and fragmentation of particles. This phenomenon was most apparent in the

top layer of sample 3. The D_F of top layer of sample 3 was much higher than the D_F of sample 2 even though number of blows applied to each was same. Although it was not as apparent as with the top layer, it can still be seen that the D_F of the middle layer of sample 3 had a higher D_F than the middle layer of sample 2 due to the greater number of contacts between particles that caused abrasion.

On the other hand, the D_F of the bottom layer of sample 3 was lower than the D_F of the same layer of sample 2. The migration of the fines during the test could have caused this high D_F in sample 2. As mentioned in the previous section, the large void space in sample 2 could have caused more particles to move down to bottom layer during the test.

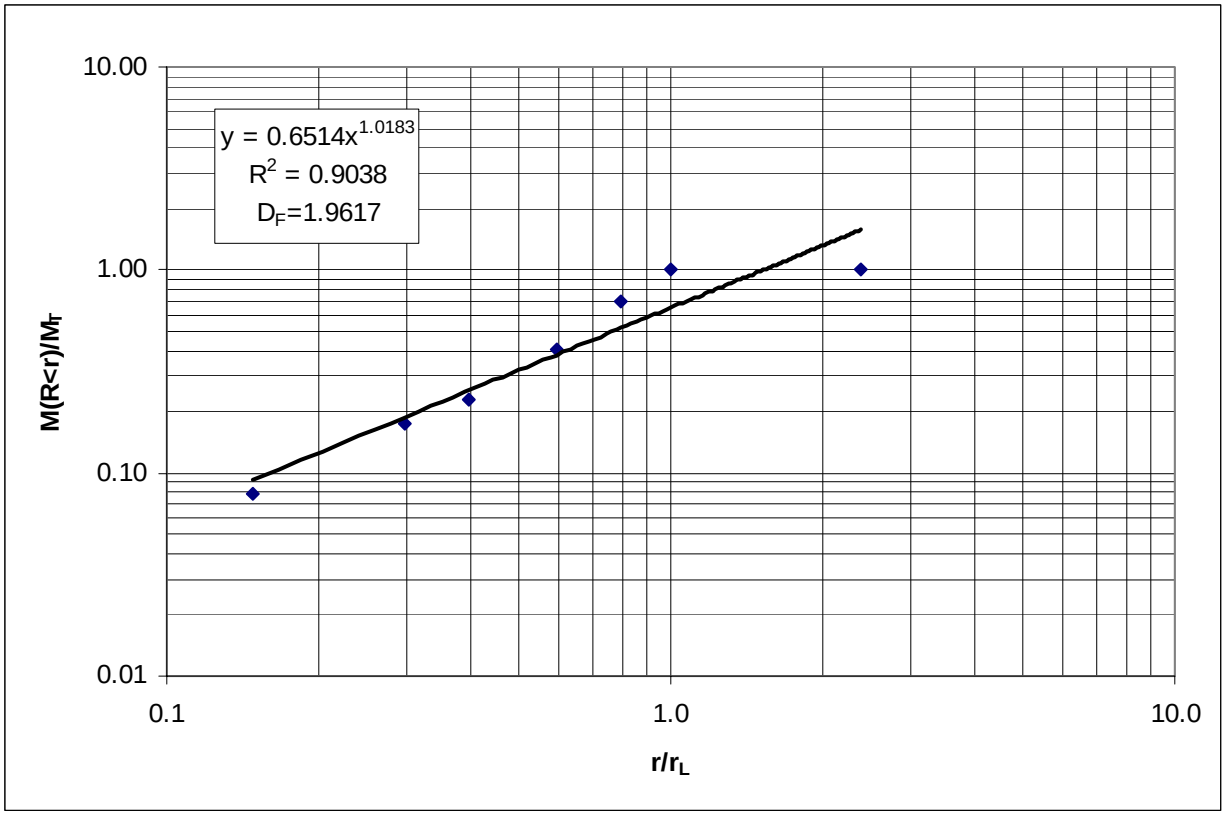

Figure 7.25: D_F of top layer of sample 3 after the test.

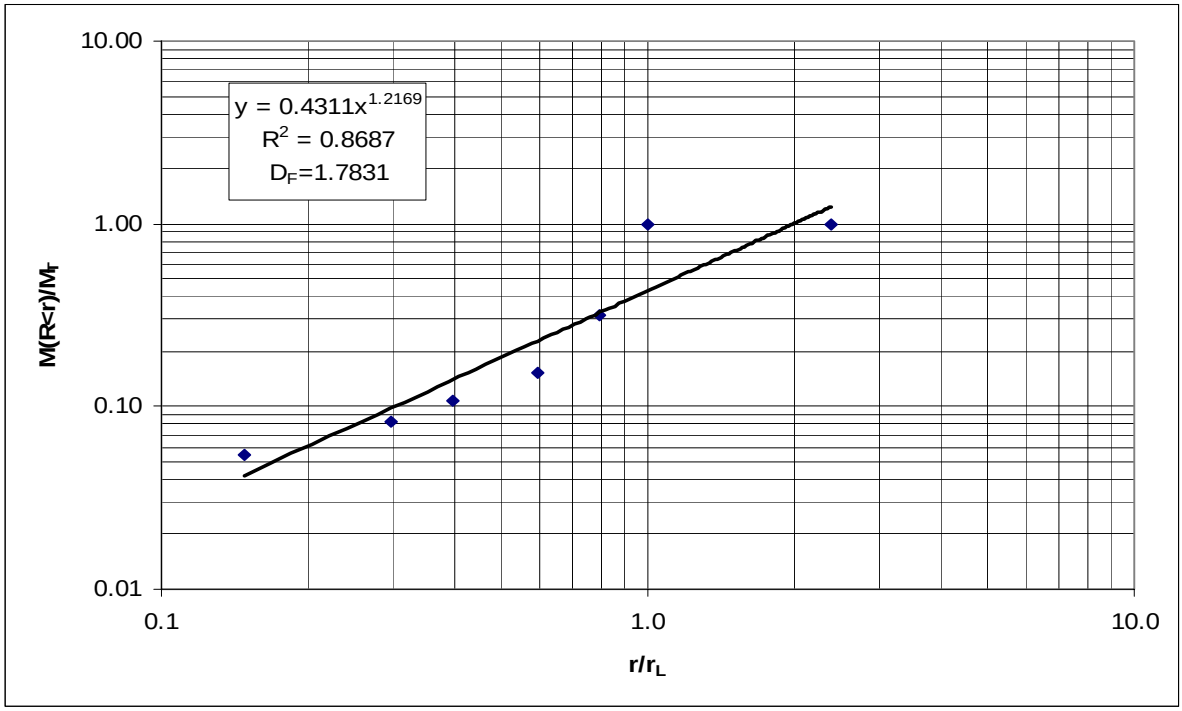

Figure 7.26: D_F of middle layer of sample 3 after the test.

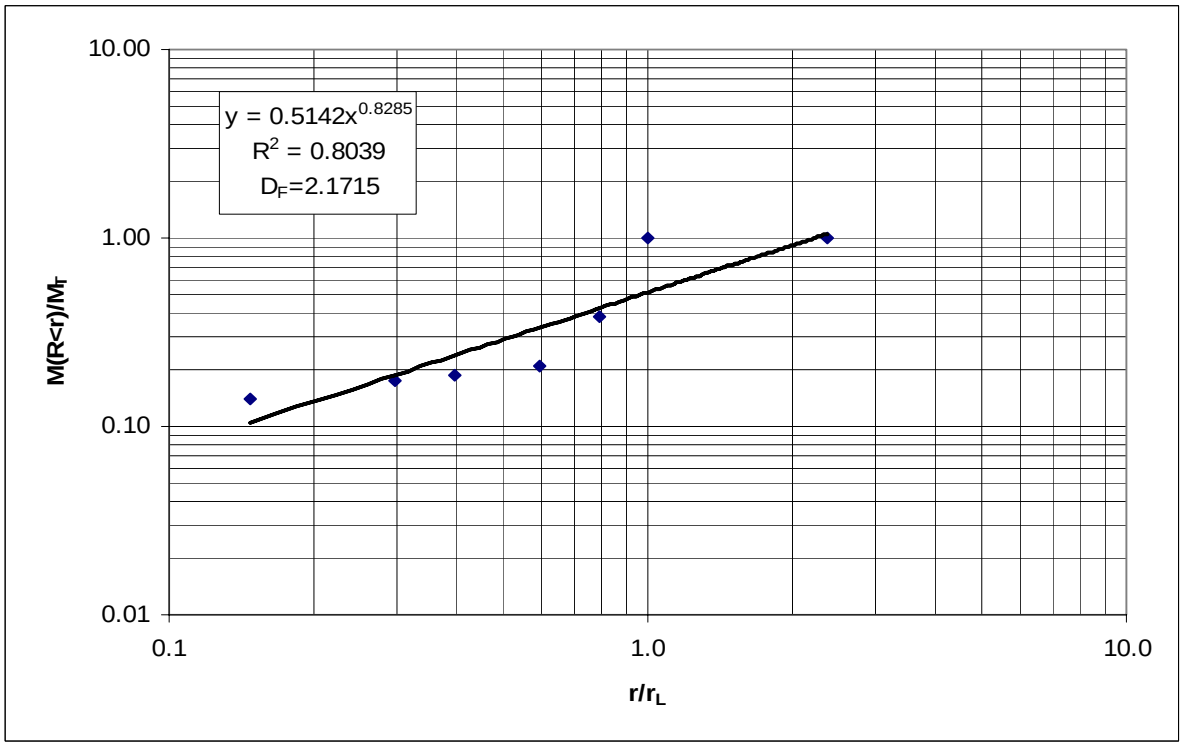

Figure 7.27: D_F of bottom layer of sample 3 after the test.

7.5 ROUGHNESS FRACTAL DIMENSION, D_R

The roughness fractal dimension, D_R, was determined for each layer of all three samples both before and after the test. For each layer, 20 to 30 particles of various sizes were used to measure area and perimeter. The result of the D_R was summarized in Table7.3 in which it can be seen that in most layers, the D_R decreased after the test no matter what particle size or layer.

However, the range of reduction varies cases by case. For example, in sample 1, the D_R of the top layer was 1.00949 before the test and decreased to 0.99600 after the test, producing a reduction of only 0.01349. On the other hand, the D_R of the top layer of sample 2 was 1.19432 before the test and 0.98145 after the test, producing a reduction of 0.21287. And in the same manner, the D_R of top layer of sample 3 before and after the test was 1.14155 and 0.97528, respectively. The change in D_R was 0.16627, which was closer to the change of sample 2 than sample 1. There could be many factors that caused this result. The first, factor was the difference in the types of failure. In sample 1, the size of particles was varied, but sample 2 had all similar sized particles. Thus, the large particles in sample 1 could have had a greater number of contacts with the surrounding particles since there were smaller particles surrounding it. This large number of contacts helped to prevent the total failure or split of the particles. Instead of total failure, they created more abrasion or failure of asperity. As determined by the result of the point load test, total failure reduces the D_R of a particle. And it was concluded that abrasion or failure of asperity doesn't reduce D_R as much as total failure. Thus, the small number of total failures of particles may explain why the reduction of D_R was smaller in the top layer of sample 1 than in the top layers of the other two samples.

Table 7.3: Summary of roughness fractal dimension, D_R, before and after the test for three different samples.

Sample #		Top Layer	Middle Layer	Bottom Layer
Sample 1	Before	1.00949	0.99256	1.06253
Sample 1	After	0.99600	1.01384	1.00276
Sample 2	Before	1.19432	1.01698	0.91950
Sample 2	After	0.98145	0.96956	0.98838
Sample 3	Before	1.14155	1.13908	1.13669
Sample 3	After	0.97528	1.01031	0.99374

The result of the middle layer of sample 1 and the bottom layer of sample 2 were the only two cases in which the roughness of particles in that layer increased after the test. From the previous analysis of grain size distribution and D_F, it was determined that the middle layer experienced the least amount of crushing in all the samples. Thus, this small increase of D_R in the middle layer of sample 1 could be due to both the small number of abrasions, which could have caused the surface to get little more uneven and to very small amount of total failure. Unlike sample 1, the D_R of the middle layer of the other two samples was reduced. The coordination number of each particle in the middle layer of sample 2 and sample 3 must be lower than that of sample 1 because all the samples were of a similar size, so the concentrated force could have raised the chance of a total failure or split particle more than with the middle layer of sample 1. Consequently, the roughness decreased in the middle layer of these two samples. However, in the case of the bottom layer of sample 2, this theory should not be applied because the D_R of the bottom layer of sample 2 before the test was determined as 0.91950, which was very small compared to other result. Thus, it was not surprising that the D_R increased after the test. Before the test, the D_R of this layer was determined twice using different pictures of the same particles

to see if there was an error during the process, but similar results were obtained. Further study is required to understand the reason for this low D_R.

7.6 SUMMARY

By dividing the samples into three layers, many characteristics of the behavior of granular material were observed, characteristic which could not have been found with the regular proctor test reported in the previous chapter. First of all, from the grain size distribution of the three samples and from Table 7.2, the characteristic of abrasion was found. The abrasion of particle was most influenced by the number of blows applied to the sample. Additional factors such as the original size of the particle could have had some influence on the degree of abrasion, but the number of blows appeared to be the key factor. Second, from the result of the grain size distributions and fragmentation fractal analysis of each layer of the three samples, it was found that the top layer always sustained the greatest amount of crushing and that the middle layer sustained the least. It was determined that there were few reasons for this phenomenon. First of all, the force that was applied to particles on the top layer was concentrated on one point. On the other hand, the force applied to particles in the middle layer was more distributed because there was more than one source of force transferring force to particles in the middle layer from particles above. The bottom layer also had more than one source of force, but the particles in the bottom layer had fewer contacts to support that force. Thus, it was determined that the top and bottom layers were in similar situations. The only difference between them was that the contacts transferring the force to the particle and the contacts supporting the particle was switched or

inversed. From the figure of the force chain produced by DEM, it was determined that some of the force was transferred to the mold and didn't reach to the bottom layer, so the bottom layer sustained less crushing than the top layer.

The analysis of the roughness fractal dimension, D_R, pointed out one especially important point, which was the relationship of roughness and the coordination number. First, it was observed that the reduction of D_R occurred in most cases, but the degree of reduction was different from case to case. The top layer of sample 1 had less reduction of D_R compared to the other two samples. This was due to a higher coordination number that the particles had in sample 1. Sample 1 had a variety of particle sizes so it had higher coordination number than the other two samples. This greater coordination number reduced the chance of total failure occurring in the particle. And since the total failure reduces the particle roughness more than abrasion or failure of asperity, the reduction of D_R was less in the top layer of sample 1 than in the other two samples. The middle layer of sample 1 experienced little increase in D_R. This was also due to the coordination number. Since the coordination number was higher in sample 1 than in the other two samples, there was less total failure even though more abrasion occurred. The small amount of abrasion and total failure could have made the surface of the particle rougher and DR of the middle layer of sample 1 increased slightly.

Finally, also, it must be noted that the D_R of the bottom layer of sample 2 before the test had a low value of that could not be explained and that further study of fractal analysis and its applicability are recommended

8.0 CONCLUSION

The data of formation of force chain under normal and shear stresses and fragmentation of granular material was presented in forgoing sections. Based on this data and analysis of this data following conclusion have been made.

- Formation of force chain was studied by using different types of wooden sticks. It was found that the formation of force chains is influenced not only by the magnitude of the applied stress but also by the type of stress. When material is only under normal stress, an arch forms on top of the location where the loose sticks are originally located. When material is under the normal and shear stress, the arch forms at bottom right section of sample. However, when the large stress is applied, arch doesn't form.
- From the results of test and DEM it was found that when normal and shear stresses are applied, the majority of the force chains form diagonally from top right to bottom left, which is the same direction as direction of sum of normal and shear stress. But when there are large number of particles, formation of force chain become complex and some force chains forms toward bottom right.
- It was found that when the large amount of shear stress is applied, the vertical deformation of sample is small despite the large normal stress.
- It was concluded that strength of granular material decreases as the diameter of the particle increases. The presence of flaw in the body of the granular material causes this reduction of strength.

- It was also concluded that the strength of granular material decreases when it is saturated. This is due to the loss of suction. The suction produced by small amount of water in the granular body increases the strength of the granular material in significant degree but when granular material is saturated, this suction can not be produced. Another factor that causes this phenomenon is the softening of mineral, which cements sand particles together, by saturation.
- From the fractal analysis it is found that the failure surface created by total failure decreases the roughness of particle because this surface is much smoother than original surface in both texturally and structurally.
- The influence of saturation was evident in grain size distribution. From the proctor test and fractal analysis, granular material was found to be subjected to more crushing when it was saturated and it was also found roughness of granular material is also influenced by saturation. The granular material becomes ductile when it is saturated and the resulting failure surface tends to be smoother than dry material.
- By dividing the samples into three layers, many characteristics of the behavior of granular material were found. It was found that the top layer always sustained most crushing and that the middle layer sustained the least. The coordination number is the important factor to explain this. The particles in middle layer had higher coordination number than top layer, so the stress transferred to particles in middle layer was distributed. On the other hand, the particles in top layer had one concentrated stress applied to their body; thus leading to lower chance of survival.
- As expected the fractal analysis was found to be very useful tool to identify roughness and size distribution of granular material. Fragmentation fractal dimension, $D_{F,}$ uncovered

the things that could not be found from grain size distribution alone. Although it calculated one unexpected value, the roughness fractal dimension, $D_{R,}$ was also found to be very useful.

BIBLIOGRAPHY

1. Pinson, D., Zou, R. P., Yu, A. B., Zulli, P., and McCarthy, M. J., "Coordination Number of Binary Mixtures of Spheres", Journal of Physics D, Applied Physics, 31, (1998), pp.457-462.

2. Mcdowell, G. R., and Bolton, M. D., "On the Micromechanics of Crushable Aggregates", Geotechnique, 48, (1998), pp.667-679.

3. Lade, P. V., Yamamuro, J. A., and Bopp, P. A., " Significance of Particle Crushing in Granular Materials", Journal of Geotechnical Engineering, April, (1996), pp.309-316.

4. Nakata, Y., Hyde, A. F. L., Hyodo, and M., Murata, H., "A Probabilistic approach to Sand Particle Crushing in the Triaxial Test", Geotechnique, 49, (1999), pp.567-583.

5. Hyslip, J. P., and Vallejo, L. E., "Fractal Analysis of the Roughness and Size Distribution of Granular Materials", Engineering Geology, 48, (1997), pp.231-244.

6. Gori, U., and Mari, M., "The Correlation Between the Fractal dimension and Internal Friction Angle of Different Granular Materials", Soils and Foundations, 41(6), (2001), pp.17-23.

7. Bowman, E. T., Soga, K., and Drummond, T. W., "Particle Shape Characterization using Fourier Analysis", CUED/D-Soils, TR315, (2000).

8. Hyslip and Vallejo, op. cit.

9. Idem.

10. Idem.

11. Idem.

12. Cundall, P. A., and Strack, O. D. L., "A Discrete Numerical Model for Granular Assemblies", Geotechnique, 29(1), (1979), pp.47-65.

13. Lobo-guerrero, S., and Vallejo, L. E., “DEM Evaluation of Granular Crushing Under Direct Shear Test Conditions”, ASCE Journal of Geotchnical and Geoenvironmental Engineering, (Not Published yet)

14. Welsh, R. A., Vallejo, L. E., Lovell, C. W., and Robinson, M. K., “Proposed Strength-Durability Classification System”, The U.S. Office of Surface Mining (OSM).

15. Hawkins, A. B., and McConnell, B. J., “Sensitivity of SandStone Strength and Deformability to Changes in Moisture content”, Quarterly Journal of Engineering Geology, 25, (1992), pp.115-130.

16. West, G., “Effect of Suction on the Strength of Rock”, quarterly Journal of Engineering geology”, 27, (1994), pp.51-56.

17. Dyke, C. G., and Dobereiner. L., “Evaluating the strength of Sandstones”, Quarterly Journal of Engineering Geology, 24, (1991), pp.123-134.

18. Billam, J., “Some Aspects of the Behaviour of Granular Materials at High Pressures”, Stress Strain Behavior of Soils, (1971), pp.69-80

19. Hawkins and McConnell, op. cit.

20. Billam, op. cit.

21. Lobo-guerrero, S., Vallejo, L., E., and Vesga, L., “Visualization of Crushing in Granular Materials Using DEM”, International Geomechanics, (Not Published yet)

22. Hyslip and Vallejo, op.cit.